inorganics

MDPI

Review

Molecular $S = 2$ High-Spin, $S = 0$ Low-Spin and $S = 0 \rightleftarrows 2$ Spin-Transition/-Crossover Nickel(II)-Bis(nitroxide) Coordination Compounds

Takayuki Ishida *, Saki Ito, Yuta Homma and Yukiya Kyoden

Department of Engineering Science, The University of Electro-Communications, Chofu, Tokyo 182-8585, Japan; ito@ttf.pc.uec.ac.jp (S.I.); homma@ttf.pc.uec.ac.jp (Y.H.); kyoden@ttf.pc.uec.ac.jp (Y.K.)

* Correspondence: takayuki.ishida@uec.ac.jp; Tel.: +81-42-443-5490; Fax: +81-42-443-5501

Abstract: Heterospin systems have a great advantage in frontier orbital engineering since they utilize a wide diversity of paramagnetic chromophores and almost infinite combinations and mutual geometries. Strong exchange couplings are expected in 3d–2p heterospin compounds, where the nitroxide (aminoxyl) oxygen atom has a direct coordination bond with a nickel(II) ion. Complex formation of nickel(II) salts and *tert*-butyl 2-pyridyl nitroxides afforded a discrete 2p–3d–2p triad. Ferromagnetic coupling is favored when the magnetic orbitals, nickel(II) dσ and radical π*, are arranged in a strictly orthogonal fashion, namely, a planar coordination structure is characterized. In contrast, a severe twist around the coordination bond gives an orbital overlap, resulting in antiferromagnetic coupling. Non-chelatable nitroxide ligands are available for highly twisted and practically diamagnetic complexes. Here, the Ni–O–N–$C_{sp}{}^2$ torsion (dihedral) angle is supposed to be a useful metric to describe the nickel ion dislocated out of the radical π* nodal plane. Spin-transition complexes exhibited a planar coordination structure in a high-temperature phase and a nonplanar structure in a low-temperature phase. The gradual spin transition is described as a spin equilibrium obeying the van't Hoff law. Density functional theory calculation indicates that the energy level crossing of the high- and low-spin states. The optimized structures of diamagnetic and high-spin states well agreed with the experimental large and small torsions, respectively. The novel mechanism of the present spin transition lies in the ferro-/antiferromagnetic coupling switch. The entropy-driven mechanism is plausible after combining the results of the related copper(II)-nitroxide compounds. Attention must be paid to the coupling parameter J as a variable of temperature in the magnetic analysis of such spin-transition materials. For future work, the exchange coupling may be tuned by chemical modification and external stimulus, because it has been clarified that the parameter is sensitive to the coordination structure and actually varies from $2J/k_B = +400$ K to -1400 K.

Keywords: aminoxyl; exchange interaction; spin crossover; structural transition; switching behavior; magneto-structural relationship

Citation: Ishida, T.; Ito, S.; Homma, Y.; Kyoden, Y. Molecular $S = 2$ High-Spin, $S = 0$ Low-Spin and $S = 0 \rightleftarrows 2$ Spin-Transition/-Crossover Nickel(II)-Bis(nitroxide) Coordination Compounds. *Inorganics* **2021**, *9*, 10. https://doi.org/10.3390/inorganics9020010

Received: 21 December 2020
Accepted: 13 January 2021
Published: 20 January 2021

1. Introduction

Various magnetic switches operative in solid states are of great interest for applications to display, memory, sensor, and related smart devices [1–8]. Structural transformations in solid states often induce a change of a number of physical properties, including magnetic, chromic, and electric properties, associated with a change of the unit cell volume, crystal/molecular symmetry and chirality, electronic state, and spin states. Heterospin systems have a great advantage in frontier orbital engineering since they utilize a wide diversity of paramagnetic (open-shell) chromophores and almost infinite combinations and mutual geometries. Organic radical species can work as ligands [6–8], and Gatteschi et al. have proposed the versatile "metal–radical approach," where considerable magnetic exchange interaction occurs through direct metal–radical coordination bonds [9,10]. Resultant short spin–spin distances and paramagnetically dense systems are favorable for

constructing strongly exchange-coupled materials and magnets. Recent works on metal–organic frameworks are making progress in materials involving a radical host and/or guest [11,12]. Multi-nuclearity and -dimensionality are important keywords in the field of molecule-based materials chemistry [13–17].

A reversible spin transition between low-spin (LS) and high-spin (HS) states triggered by external stimuli such as heat and light is named spin crossover (SCO) [1–5,16–19]. Iron(II) ($3d^6$) compounds are the most popular [20–28], since magnetic and chromic changes are drastic between $S = 0$ diamagnetic and $S = 2$ paramagnetic states. Furthermore, considerable attention has been paid to room-temperature SCO [29] required for applications under ambient conditions. Multi-functional SCO materials are also attracting much attention, for example, exchange-coupled [30] and mesophase-related materials [31–33].

In spin-transition phenomenon, LS states are favored for the enthalpy control in a low-temperature phase, whereas HS states for the entropy control in a high-temperature phase [34,35]. As Figure 1 depicts, the Gibbs energy of a HS state tends to be low-lying in a high-temperature phase due to an enhanced entropy term in $G = H - TS$. Entropy as a coefficient of temperature becomes larger when a spin multiplicity is higher, because the degeneracy $2S + 1$ contributes to the entropy by $nR \ln(2S + 1)$. The critical temperature T_c is defined with the energy-level crossing between the HS and LS states. Spin-transition behavior would take place only under limited conditions, where the energy levels of HS and LS states are close to each other.

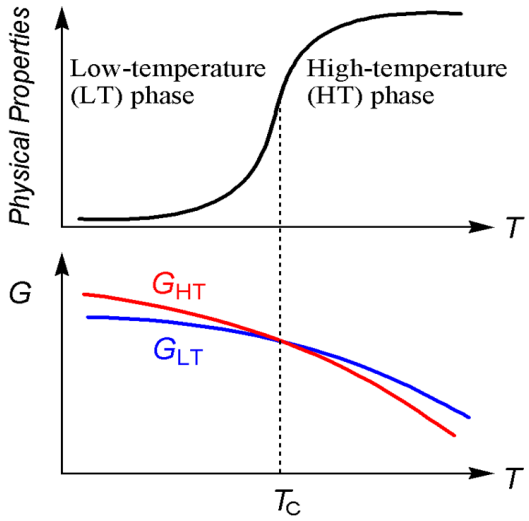

Figure 1. Schematic drawings of (**top**) physical properties (the product $\chi_m T$ for example) as a function of temperature and (**bottom**) Gibbs energy diagram for phase transition materials.

A major subject of this review is to describe a successful application of the magneto-structural correlation to development of molecular HS, LS, and novel spin-transition compounds in nickel(II)($3d^8$)-bis(nitroxide) heterospin systems. While exotic spin-transition/-crossover systems have been explored extensively [6,36,37], we will report here the $S = 0 \rightleftarrows 2$ spin-transition system other than iron(II) complexes. We have utilized nitroxides or aminoxyls as a 2p spin source, because nitroxides are persistent enough when sterically bulky and/or π-conjugate substituents are attached at appropriate positions [38,39]. Nitroxides are highly accessible and chemically modifiable in many ways [40–45], and actually various spin label agents, such as TEMPO and PROXYL, are commercially available and derivatized by users [39,40,46,47]. The new nickel(II)-bis(nitroxide) coordination compounds of the present work were synthesized in a rational manner, since the molecules are designable. The chelate ring size is programmable in particular. After overviewing the various ground states in nickel(II)-bis(nitroxides), the transition can be assumed just as an entropy-driven SCO phenomenon, which is highlighted in this review.

There are a few reports on related spin-transition in 3d–2p heterospin systems. Though the present review is focused on nickel(II)–nitroxide systems, some relevant copper(II)–nitroxide systems have already been known, and we have to check them out. Ovcharenko et al. intensively explored the spin-transition materials in copper(II)($3d^9$)–nitroxide compounds as named "breathing crystals" [48–50]. The mechanism has been originally proposed by Rey et al., which involves a switch of the role of axial and equatorial coordinations [51,52]. It works only in octahedral copper(II) systems having the magnetic orbital in a basal plane. In contrast, our group focused on octahedral nickel(II) complexes, where the magnetic orbitals are localized both in $3d_{z^2}$ and $3d_{x^2-y^2}$. A coupling switch actually takes place at any coordination sites, axial or equatorial. Another advantage of our system is strong ferromagnetic coupling, often stronger than the order of a thermal energy at room temperature.

Rey et al. also reported another type of spin transition in copper(II)–nitroxide materials [53]. The copper(II) coordination environment is changed between a trigonal bipyramid and a square pyramid. This mechanism utilized the five-coordinate environment, and it would be limited practically only for copper(II) compounds. Their compounds were regarded as a "pseudo-spin-transition" material displaying an alteration between strong and weak ferromagnetic couplings. According to their classification, "genuine spin-transition" materials that would serve a ferro-/antiferromagnetic coupling switch are the target of our project.

2. Results and Discussion

2.1. Advantage of Nitroxides

Heterospin strategy takes advantage of a variety of the symmetry and energy level of magnetic orbitals. The exchange interactions in heterospin compounds have been intensively investigated in connection with molecular structures [9,10,54–58], because they are regulated as well with their mutual spatial arrangement. McConnell has proposed that the exchange interaction is proportional to the spin densities at the interacting atoms [59]. Accordingly, a paramagnetic center atom is directly bonded to a metal center, giving rise to considerable exchange coupling.

There have been a number of organic (2p) spin carriers and related tailored ligands owing to sophisticated synthetic techniques. For example, SQ, NN, IN, VD, DTDA, and BT are well-known persistent radicals (Figure 2), usually carrying a π* spin. A 2-pyridyl group (abbreviated as 2py, hereafter) or related 2-azaaromatic ring was introduced as Ar in Figure 2. Namely, 2,2′-bipyridine-6,6′-diylbis(NN) [60], 2pyIN [61,62], 2pyVD [63], 2pyDTDA [64,65], and 2pyBT [66,67] are ready to form a chelated structure in the presence of transition metal ions. The benzotriazinyl or Blatter's radical (BT) [68] is a relative newcomer [66] in the community of the 2p–3d heterospin molecular magnetism. When copper(II) and nickel(II) ions were applied, ferromagnetic couplings were often observed (see below).

The discovery of the ferromagnetic coupling in copper(II)- and nickel(II)-SQ compounds by Kahn [69] and Benelli [70] is recognized as a pioneering work. These works are important for the progress of ferromagnetic heterospin systems in materials chemistry and also for comprehension of the nature of exchange interaction in terms of theoretical quantum chemistry. Moreover, SQ derivatives and their aza analogues have established the foundation for the development of valence tautomeric compounds [71–73]. The spin density at the ligating atom is reduced owing to spin delocalization onto the wide heteroatomic system: N_2O_2 in NN, N_2O_1 in IN, N_4 in VD, N_2S_2 in DTDA, and N_3 in BT. Compared with these radicals, we assume that aryl *tert*-butyl nitroxides (Ar–NO; the *tert*-butyl nitroxide group is abbreviated as NO hereafter) would have an advantage; the nitroxide group has a relatively large spin density on the ligating oxygen atom [74], as proven with the ESR, NMR, and polarized neutron diffraction experiments. Iwamura et al. have explored the bulk magnets comprising HS di- and trinitroxides and magnetic transition metal ions [8]. The coordination ability of nitroxide oxygen atoms has been noticed since 1970's [9].

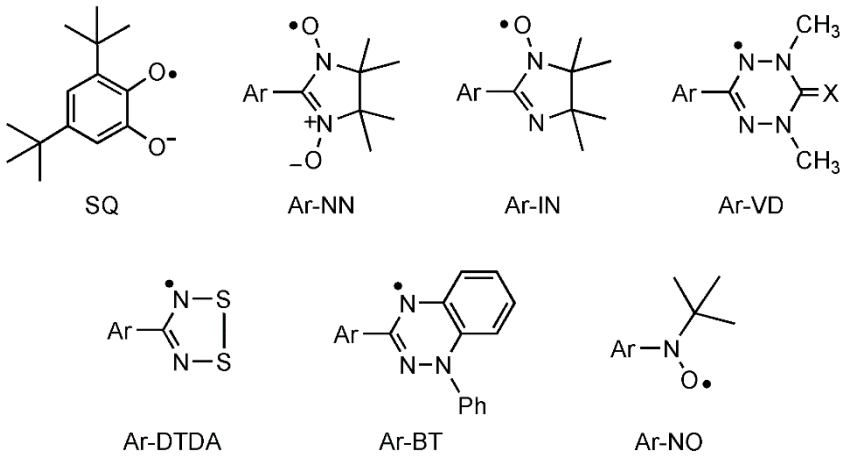

Figure 2. Structural formulas. Abbreviations: SQ, semiquinonate; NN, nitronyl nitroxide; IN, imino nitroxide; VD, verdazyl; DTDA, dithiadiazolyl; BT, benzotriazinyl; NO, *tert*-butyl nitroxide.

2.2. Magneto-Structural Relationship and Molecular Design

Copper(II)– and nickel(II)–radical complexes having a direct radical coordination bond are the best documented in the 3d–2p heterospin systems [9,60–70]. There have been an increasing number of compounds showing a ferromagnetic 3d–2p coupling [75–81]. It is believed for a long time that axial coordination in copper(II)–nitroxide complexes displays relatively weak ferromagnetic interaction whilst equatorial coordination strong antiferromagnetic interaction [9]. However, after the accumulation of experimental results, it becomes familiar that ferromagnetic interaction is possible in equatorial coordination [60–62]. On the contrary, the magnitude of the coupling interactions often exceeds the order of thermal energy of room temperature, even in the ferromagnetic case. The following explanation is plausible [69,74]. Strictly orthogonal arrangement of two magnetic orbitals (metal dσ and radical π*) favors ferromagnetic coupling (Figure 3a,c). In contrast, severe twist around the coordination bond gives rise to an orbital overlap between magnetic orbitals and consequently antiferromagnetic interaction (Figure 3b,d). This mechanism is operative, regardless of the equatorial or axial sites of nickel(II) coordination environments, which is different from that of some other copper(II)–radical case regulated with a different mechanism [48–53] (see Section 1).

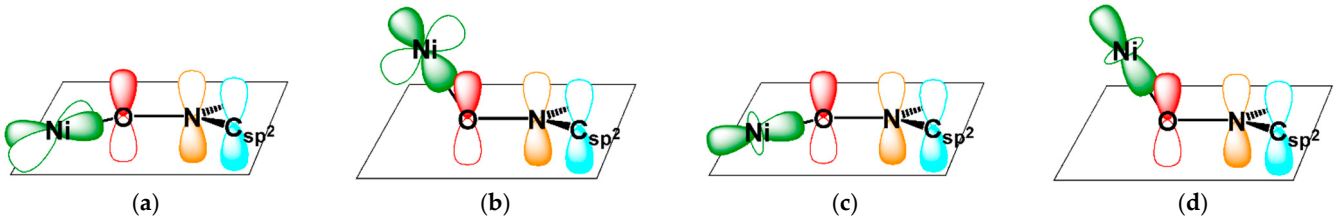

Figure 3. Arrangement of atomic orbitals, (**a**,**b**) Ni($3d_{x^2-y^2}$)–O($2p_z$)–N($2p_z$)–C_{sp^2} ($2p_z$) and (**c**,**d**) Ni($3d_{z^2}$)–O($2p_z$)–N($2p_z$)–C_{sp^2}($2p_z$). The Ni ions are (**a**,**c**) located on the π* nodal plane and (**b**,**d**) dislocated out of the plane. This picture is also applicable to other conventional organic radical ligands having a well-defined π* nodal plane.

Depending on whether the interaction is antiferro- or ferromagnetic, the molecular spin state is called HS (the magnetic moments add up) or LS (the magnetic moments compensate each other). In this review, the local metallic spin states are unchanged; $S_{Ni}^{2+} = 1$ and $S_{Cu}^{2+} = 1/2$ in the HS and LS states and throughout possible spin transition.

Five-membered chelate rings seem to have advantage for the planar conformation over 6-membered ones. A 5-membered chelate has a relatively open bite angle with respect to ligating atoms and force to flatten the chelate ring. In fact, as Luneau et al. reported [61], the copper(II) and 2pyIN complex possessed a 5-membered chelate ring and ferromagnetic coupling with $2J/k_B = +420$ K, and the planar conformation is indicated with the Cu–N–

C–C_{sp}^2 torsion (φ) of 1.0°. Here, the exchange coupling parameter J is defined in the $\hat{H} = -2J\hat{S}_1 \cdot \hat{S}_2$ convention. In this regard, we have to stress that 2-azaaryl-NO ligands would be one of the best candidates for exploring ferromagnetic complexes, because coordination compounds with 2-azaaryl-NO always involve a 5-membered chelate ring. In contrast, the corresponding 2pyNN derivative having a 6-membered chelate ring is likely to undergo out-of-plane distortion and actually displays antiferromagnetic couplings [82,83]. Some exceptions have been reported; the complex from nickel(II) and 4-imidazolyl-NN exhibited a ferromagnetic coupling of $2J/k_B$ = +85(3) K [84,85]. In that case, the small imidazole ring may force the O and N bite angle open in the 6-membered ring. Thus, the relatively planar chelate indicated with the Ni–O–N–C_{sp}^2 torsion angle of 6.3(4)° is reasonably acceptable. A quite similar synthetic strategy has been adopted to the copper(II) perchlorate and 2-imidazolyl-NN complex, which showed $2J/k_B$ = +216 K [86,87]. The nickel(II) analogue was also reported to show ferromagnetic coupling [87]. Another type of exception is found in the nickel(II)-2,2′-bipyridine-6,6′-diylbis(NN) complex [60]. The highly planar structure may be associated with the presence of three tandem chelate rings, one of which is a 5-membered ring involving a bpy (2,2′-bipyridine) moiety.

The choice of a geometrical parameter is key to easy comprehension of the mutual spatial arrangement of magnetic orbitals. Based on the above experimental results, $|\varphi$ (M–O–N–C_{sp}^2)$|$ is chosen as a handy metric [74,88,89]. Here, the torsion angle is defined by a dihedral angle between the M–O–N and O–N–C_{sp}^2 planes, as depicted in the inset of Figure 4. A plot of J vs. $|\varphi|$ for the octahedral copper(II) and nickel(II) complexes was drawn, and a distinct correlation appears (Figure 4).

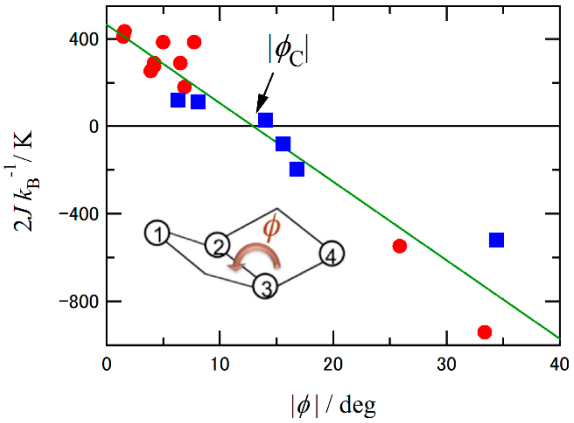

Figure 4. A plot of the exchange coupling parameter (2J) vs. $|\varphi$ (M–O–N–C_{sp}^2)$|$ in the octahedral nickel(II) and copper(II) complexes with nitroxide (red circles) and nitronyl nitroxide ligands (blue squares) (NO and NN, respectively, in Figure 2). The source of these data has appeared in References [74,88–90]. A solid line stands for a linear fit. Inset shows a schematic drawing of φ defined in the atomic sequence 1-2-3-4.

The φ parameter in M–O–N–C_{sp}^2 implies the degree of the out-of-plane dislocation of M from the π*nodal plane defined by three sp^2-hybridized atoms O, N, and adjacent C_{sp}^2 in the ligand. Syn- and antiperiplanar limits correspond to φ = 0 and ±180°, respectively, as ideal in-plane coordination structures. We can simply call this to be "planar." The plus/minus sign of φ means a chirality on the torsion. The absolute values are important in the discussion of the following sections. Eventually, this formalism (Figure 4) entirely satisfies the exchange mechanism proposed (Figure 3). The critical $|\varphi_C|$, where the sign of J alters from positive to negative, is optimized to 12.8(8)° [74,89]. After the data on the copper(II) and nickel(II) complexes are separated, $|\varphi|$ for the nickel(II) category became 21(1)° from the linear fit or 26(3)° from the cos(2φ) fit [91,92]. Thus, the magnetic coupling becomes predictable from the molecular structure.

Theoretical background for the magneto-structural relationship is as follows. The observable exchange interaction comprises ferro- and antiferromagnetic contributions as

written in Equation (1), according to Kahn's approach [54]. The J_F term arises from the two-electron exchange integral (Equation (2)), which is always positive. The J_{AF} term is regulated with the overlap and transfer integrals between the two magnetic orbitals (Equation (3)), which is negative [93–95].

$$J_{obs} = J_F + J_{AF} \quad (1)$$

$$J_F = 2K \quad (2)$$

$$J_{AF} = 4\beta S \quad (3)$$

An intercept at $\varphi = 0$ (Figure 4) stands for the J_F term as a ferromagnetic limit, and a decrease accompanied by a slope for the J_{AF} term as an angular dependence. This is why both ferro- and antiferromagnetic cases can be discussed on the same ground. The magnitude of orbital overlap is sensitive to the torsional configuration, and antiferromagnetic contribution is overwhelmingly large in general. As a result, ferromagnetic coupling would survive only when the magnetic orbitals are arranged in a strictly or very closely orthogonal manner.

In the following sections, we will describe several kinds of nickel(II)–nitroxide coordination complexes developed by our group. The 3d and 2p spins are correlated within a molecule, but the molecules are magnetically isolated in a crystal. First, ground HS molecules are demonstrated as a successful example according to the molecular design described here. Almost ideal planar coordination structures give a ferromagnetic limit (Section 2.3). Second, spin-transition (Section 2.4) and unfinished ("pseudo") spin-transition molecules (Section 2.5) are elaborated, and a *co*-ligand dependence on the transition temperature will be discussed. Finally, ground LS molecules are shown as an almost ideal antiferromagnetic limit (Sections 2.6 and 2.7).

2.3. High-Spin Molecules

Complex formation of nickel(II) salts with aryl *tert*-butyl nitroxides afforded a 2p–3d–2p triad as a discrete molecule. Figure 5 shows the structural formulas of several 2pyNO-based derivatives. A bulky substituent on the Ar ring improves persistency of the radicals under ambient conditions.

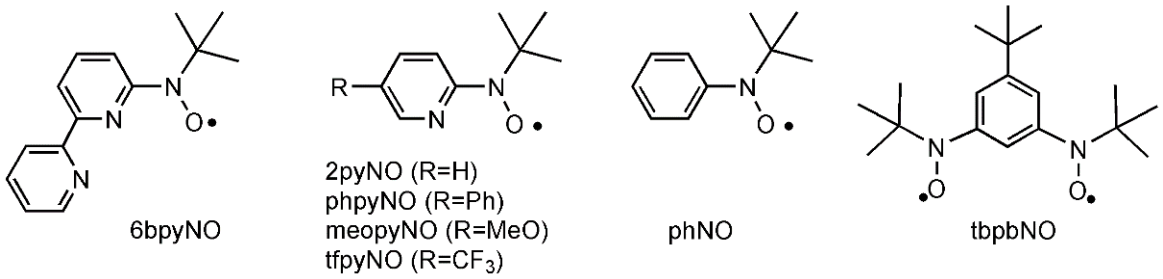

Figure 5. Structural formulas of 2pyNO derivatives and related compounds.

Figure 6a shows the complex cation portion in $[Ni(6bpyNO)_2](PF_6)_2$ [96] having two meridional 6pbyNO ligands. The two ligands are crystallographically independent. Furthermore, there are two independent molecules in a unit cell. The Ni–O and Ni–N distances in 2.084(3)–2.100(3) and 1.965(3)–2.086(4) Å, respectively, form an octahedral environment around the nickel(II) ion, guaranteeing that each nickel ion has $S_{Ni}^{2+} = 1$. The Ni-O–N–C_{sp}^2 torsion angles were 4.8(4), 5.5(5), 4.6(5), and 4.9(5)°. These small torsion angles imply the planar structure of the chelate ring. The tandem 5-membered chelates are supposed to be just suitable for the coplanar coordination structure.

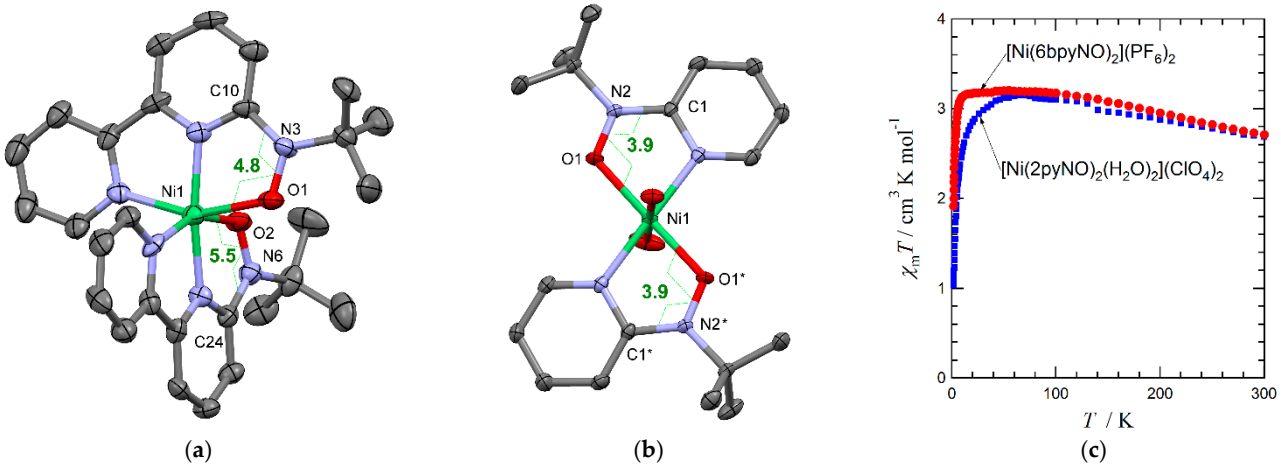

(**a**) (**b**) (**c**)

Figure 6. X-ray crystal structures of (**a**) $[Ni(6bpyNO)_2](PF_6)_2$ and (**b**) $[Ni(2pyNO)_2(H_2O)_2](ClO_4)_2$, measured at 90 and 100 K, respectively. Counter anions and hydrogen atoms are omitted for the sake of clarity. Thermal ellipsoids are drawn at the 50% probability level. Selected atomic numbering and Ni–O–N–$C_{sp}{}^2$ torsion angles are indicated. (**c**) Temperature dependence of $\chi_m T$ for the two compounds. Adapted with permission from [96,97], published by the American Chemical Society, 2006 and 2007.

The mother ligand 2pyNO is known to be unisolable [98], so that the complexes were synthesized immediately after the formation of 2pyNO without isolation. The chelate rings involving 2pyNO in $[Ni(2pyNO)_2(H_2O)_2](ClO_4)_2$ [97] are depicted in Figure 6b. A two-fold axis is located at Ni1. Two water molecules occupy the axial positions, and an octahedron is characterized with the Ni–O and Ni–N distances of 2.008(2)–2.080(4) Å. The small Ni1–O1–N2–C1 torsion angle (3.9(3)°) was recorded. Even a single 5-membered chelate ring can afford a planar structure, and this finding allows us a variety of chemical modification on the 2py ring (see below).

The outline on how to comprehend the magnetic behavior is depicted in Figure 7. The theoretical $\chi_m T$ value, the product of the molar magnetic susceptibility and temperature, or the Curie constant is calculated from the spin quantum number S according to Equation (4), where the symbols have the following meanings; N_A, the Avogadro constant; μ_B, the Bohr magneton; k_B, the Boltzmann constant; g, the Landé g factor. The spin-only value with $g = 2$ can approximately be rephrased as Equation (5) in the conventional unit of the Curie constant, cm^3 K mol^{-1} [99–101]. The paramagnetic limit of multi-spin systems, where each spin center is magnetically isolated, can also be calculated. For example, a molecule comprising an octahedral nickel(II) ion ($3d^8$; $S_{Ni}{}^{2+} = 1$) and two radicals ($S_{rad} = 1/2$) has 1.75 cm^3 K mol^{-1} in total. In contrast, the HS $S_{total} = 2$ state displays 3.0 cm^3 K mol^{-1}. When g is deviated from 2, it would be helpful to recall that $\chi_m T$ is proportional to g^2.

$$\chi_m T = \frac{N_A g^2 \mu_B^2 S(S+1)}{3k_B} \quad (4)$$

$$\chi_m T/\text{cm}^3\ \text{K mol}^{-1} = S(S+1)/2 \quad (5)$$

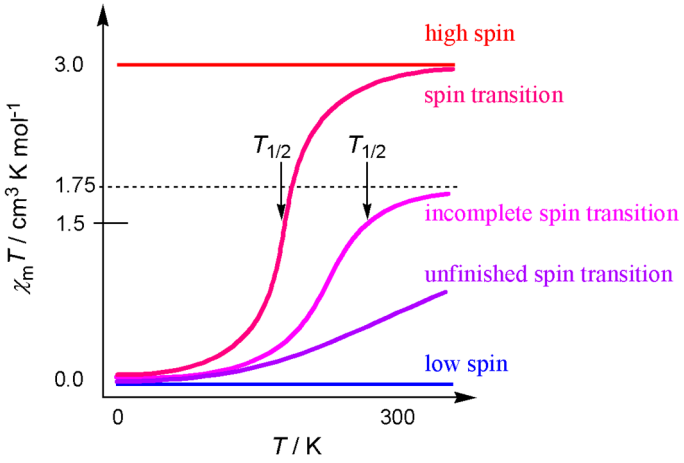

Figure 7. The spin-only values of the high-spin, low-spin, and paramagnetic limits for a symmetrical linear S_{rad}–$S_{Ni}{}^{2+}$–S_{rad} system. Classification of spin-transition behavior will be referred from Sections 2.4 and 2.5.

From the magnetic study on these compounds (Figure 6c), the $\chi_m T$ values increased upon cooling from 300 to 100 K. This finding indicates the presence of intramolecular ferromagnetic interactions in both compounds, giving the ground spin structures drawn as ↑-↑↑-↑. The $\chi_m T$ values increased up to 3.2 cm^3 K mol^{-1}, which is close to the value 3.0 cm^3 K mol^{-1} for an S_{total} = 2 species. At 300 K, the $\chi_m T$ values still exceed the spin-only paramagnetic limit (1.75 cm^3 K mol^{-1}). A symmetrical linear arrayed 3-centered model (Equation (6)) was applied to the magnetic analysis. Fitting to the resultant van Vleck equation (equation (7)) [102] afforded the optimized parameters $2J/k_B$ = +318(4) and +252(6) K for [Ni(6bpyNO)$_2$](PF$_6$)$_2$ and [Ni^{II}(2pyNO)$_2$(H$_2$O)$_2$](ClO$_4$)$_2$, respectively, after possible contribution from intermolecular antiferromagnetic coupling and nickel(II) ion zero-field-splitting effect are taken into consideration.

$$\hat{H} = -2J\left(\hat{S}_{rad1}\bullet\hat{S}_{Ni} + \hat{S}_{rad2}\bullet\hat{S}_{Ni}\right) \quad (6)$$

$$\chi_m = \frac{2N_A g_{avg}^2 \mu_B^2}{k_B T} \frac{\exp(-2J/k_B T) + 1 + 5\exp(2J/k_B T)}{\exp(-4J/k_B T) + 3\exp(-2J/k_B T) + 3 + 5\exp(2J/k_B T)} \quad (7)$$

Hence, we have clarified the first examples of nickel(II) complexes that possess highly planar Ar–NO chelate rings and at the same time show considerably strong ferromagnetic interactions (Figure 6). The exchange mechanism based on the coordination geometry (Figure 4) is plausible, and molecular design seems to be promising.

There have now been a number of instances of ferromagnetic nickel(II)–radical complexes. We have designed novel paramagnetic ligands phpyNO and meopyNO (Figure 5), in which Ph and MeO groups are introduced at the "para" position with respect to the nitroxide group for improving stability of the ligands themselves under ambient conditions. The experimental results using them are entirely compatible with the results and discussion on the mother 2pyNO complexes. From the X-ray crystallographic analysis of [NiL$_2$(H$_2$O)$_2$](ClO$_4$)$_2$, the torsion angles are 1.5(3) and 4.2(3)° for L = phpyNO (Figure 8a) and meopyNO (Figure 8b), respectively. From the magnetic study, the metal–radical ferromagnetic exchange couplings were quantified as $2J/k_B$ = +409(10) and +288(5) K, respectively [74,88]. In fact, [Ni(phpyNO)$_2$(H$_2$O)$_2$](ClO$_4$)$_2$ enjoys the status of the record holder for the strongest nickel(II)–radical ferromagnetic coupling [91].

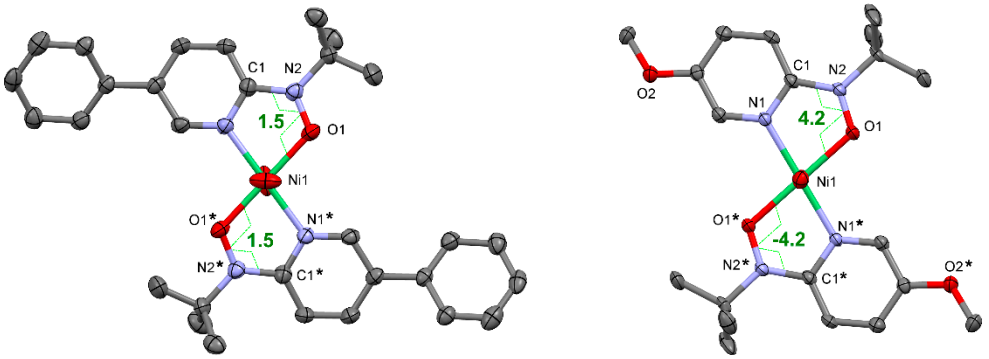

(**a**) (**b**)

Figure 8. X-ray crystal structures of (**a**) $[Ni(phpyNO)_2(H_2O)_2](ClO_4)_2$ and (**b**) $[Ni(meopyNO)_2(H_2O)_2](ClO_4)_2$ measured at 104 and 108 K, respectively. Counter anions and hydrogen atoms are omitted for clarity. Thermal ellipsoids are drawn at the 50% probability level. Selected atomic numbering and torsion angles (φ (Ni–O–N–$C_{sp}{}^2$)) are indicated. The molecules possess a two-fold symmetry for (**a**) and a centrosymmetry for (**b**). Adapted with permission from [74,88], published by the American Chemical Society, 2008 and Elsevier, 2009 for (**a**) and (**b**), respectively.

2.4. Spin-Transition Molecules

Upon these backgrounds described in Sections 2.1–2.3, we developed a novel spin-transition behavior in heterospin 2p–3d–2p triads $[Ni(phpyNO)_2X_2]$; X = Cl [103], Br [89]). In this section, the Cl derivative is focused (Figure 9), taking for an example.

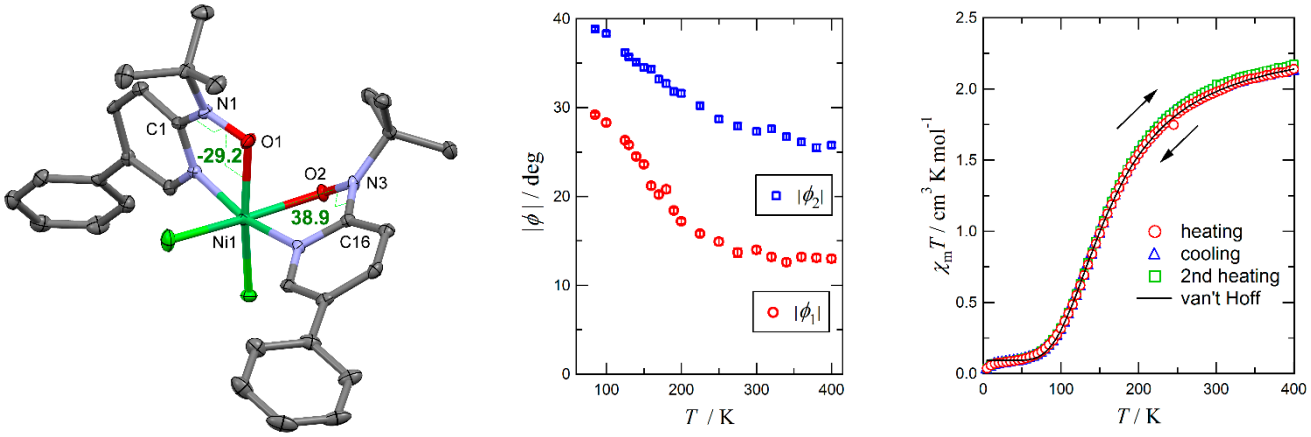

(**a**) (**b**) (**c**)

Figure 9. (**a**) X-ray crystal structures of $[Ni(phpyNO)_2Cl_2]$ measured at 85 K. Thermal ellipsoids are drawn at the 50% probability level. Hydrogen atoms are omitted. Selected atomic numbering and torsion angles (φ (Ni–O–N-$C_{sp}{}^2$)) are indicated. (**b**) Temperature dependence of torsion angles ($|\varphi|$) and (**c**) temperature dependence of $\chi_m T$ for $[Ni(phpyNO)_2Cl_2]$. Adapted with permission from [103], published by the American Chemical Society, 2018.

From the crystallographic study on $[Ni(phpyNO)_2Cl_2]$, the nickel(II) ion forms an octahedral geometry, indicating $S_{Ni}{}^{2+} = 1$ (Figure 9a). On cooling, the space group $P2_1/c$ retained, and the Ni1–O1, Ni1–O2, and other bond lengths were almost unchanged. The coordination sphere can be characterized by means of the SHAPE analysis [104], and the continuous shape measures (CShM values) are a sensitive structural indicator in many conventional one-centered SCO complexes [26,30,105,106]. The CShM values to the ideal octahedron were 1.749 at 400 K and 1.970 at 85 K for $[Ni(phpyNO)_2Cl_2]$, indicating that the crystal field hardly changes. This feature is characteristic of the spin transition materials of the present type. In contrast, the Ni–O–N–$C_{sp}{}^2$ torsions are sensitively enhanced as a function of temperature (Figure 9b). The Ni–O–N–$C_{sp}{}^2$ torsion angles are 13.0(4) and 25.8(3)° at 400 K while 29.2(2) and 38.9(2)° at 85 K. Namely, these torsions move from the

"ferromagnetic region" to the "antiferromagnetic region" (Figure 4). The breakdown of the dσ(Ni)−π*(nitroxide) orthogonal geometry will lead to antiferromagnetic interaction.

Figure 9c displays the magnetic susceptibility result of [Ni(phpyNO)$_2$Cl$_2$]. The $\chi_m T$ value at 400 K was 2.14 cm^3 K mol^{-1}, and the positive slope remained here. The extrapolated $\chi_m T$ value at the HS limit was 2.38(2) cm^3 K mol^{-1} at 400 K, which is larger than the paramagnetic limit from one nickel(II) ion and two radicals (2.14 cm^3 K mol^{-1} from $g_{Ni}{}^{2+}$ = 2.36 determined from the ESR experiments). This finding implies the ground spin structure of ↑-↑↑-↑ in the high-temperature phase. On cooling, the $\chi_m T$ value monotonically decreased, indicating the presence of strong antiferromagnetic interaction. The temperature range of this behavior coincides with that of the structural deformation (Figure 9b). The crystallographic study also rejects possibility of any intermolecular antiferromagnetic coupling. Below 50 K the specimen was practically diamagnetic (S_{total} = 0). The spin structure becomes ↓-↑↑-↓. Therefore, we can conclude that the intramolecular 3d–2p interactions undergo an exchange-coupling switch. In other words, a spin transition occurs as the whole [Ni(phpyNO)$_2$Cl$_2$] molecule. The variable-temperature X-band ESR study on polycrystalline [Ni(phpyNO)$_2$Cl$_2$] clearly supports the spin-transition behavior.

Owing to the molecular structure deformation, the exchange coupling parameter J is supposed to be a function of temperature. Therefore, the van Vleck analysis with constant exchange coupling is inappropriate and actually did not work. Although the magnetic analysis involving temperature-dependent coupling parameter was reported [53,107], no suitable expression of $J(T)$ is known for the present case. Instead, the magnetic data were found to perfectly obey the van't Hoff law (Figure 9c). The observed behavior is best described as equilibrium in a solid-state chemical reaction.

A question arises here whether the observed structure is an identical geometry or an average in time or space [108]. As the animated picture deposited as a supporting information file shows [103], the thermal ellipsoids of the oxygen atoms are normal during the transition. In the present case, every structure has an identical geometry, and magnetic properties are associated with each structure. The equilibrium model can be applied to the two terminal states.

The van't Hoff analysis is a popular method to quantify SCO behavior [34,54,109]. The original van't Hoff equation is given by Equation (8). The equilibrium constant is rewritten by using molar HS and LS fractions, γ_{HS} and γ_{LS}, respectively (Equation (9)). Putting Equation (9) into Equation (8) leads to Equation (10). The transition entropy change is related with Equation (11) because ΔG vanishes at equilibrium. The spin-transition temperature $T_{1/2}$ is defined as the temperature satisfying $\gamma_{HS} = \gamma_{LS}$, and in this treatment the phase transition temperature T_C has the same meaning of $T_{1/2}$. The $\chi_m T$ data set is converted to γ_{HS} by Equation (12), where C is the Curie constant of the HS species. Thus, the SCO temperature of [Ni(phpyNO)$_2$Cl$_2$] was calculated as $T_{1/2}$ = 173.7(8) K. Note that the error bar seems to be considerably reduced, thanks to many data points from the entire temperature range used in the statistical analysis.

$$\ln[K(T)] = \frac{-\Delta G}{RT} = \frac{-\Delta H}{RT} + \frac{\Delta S}{R} \quad (8)$$

$$K(T) = \frac{\gamma_{HS}}{\gamma_{LS}} = \frac{\gamma_{HS}}{1-\gamma_{HS}} \quad (9)$$

$$\gamma_{HS} = \frac{1}{1+exp[(\Delta H/R)(1/T-1/T_{1/2})]} \quad (10)$$

$$\Delta S = \Delta H/T_{1/2} \quad (11)$$

$$\chi_m T = C\gamma_{HS} \quad (12)$$

The experimental results on the bromide analogue [Ni(phpyNO)$_2$Br$_2$] [89] are similar. The variable-temperature crystallographic analysis indicates the structural transformation. The magnetic data obeyed the van't Hoff model, clarifying $T_{1/2}$ = 134(1) K. However,

it is a dissimilar point that the $\chi_m T$ vs. T profile exhibited a monotonic increase to the paramagnetic limit and not to the high-spin limit on heating. The $\chi_m T$ value was only 1.96 cm^3 K mol^{-1} at 400 K. In short, the HS nature is buried by a possible thermal depopulation from the HS state, even though the spin transition is almost finished. The experimental $\chi_m T$ value approaches the non-interacting limit. Therefore, we named this behavior an apparent "incomplete spin transition" (Figure 7). The origin of "incomplete" is different from that of typical iron(II) SCO materials; incomplete SCO usually takes place in a low-temperature phase [1,110]. The theoretical calculation supports this conclusion (see the next section). Thus, the new scenario of the spin transition based on the solid-phase equilibrium reaction has been established for the X = Cl and Br compounds.

We have to refer a closely related spin-transition behavior found in the corresponding copper(II) version. The mechanism includes torsional deformation around the coordination bond just like the above nickel(II) compounds. The magnetic study of $[Cu(phpyNO)_2(H_2O)_2](BF_4)_2$ [111] (Figure 10a) revealed the presence of the ferromagnetic coupling on both wings in a high-temperature region, leading to the spin structure of ↑-↑-↑ (S_{total} = 3/2). After a spin transition at 175 K, the S_{total} = 1/2 state appeared. The crystallographic analysis clarified that an out-of-plane chelate ring deformation occurred around 175 K only on one side (31.1(3)° at 94 K for Cu1–O2–N4–C16), breaking the crystal symmetry: the space groups $P2_12_12_1$ and $C222_1$ in the LS and HS phases, respectively. The spin structure of the low-temperature phase is not ↑-↓-↑, but ↑-↑-↓. Only one side transition is enough for minimization of S_{total} to 1/2.

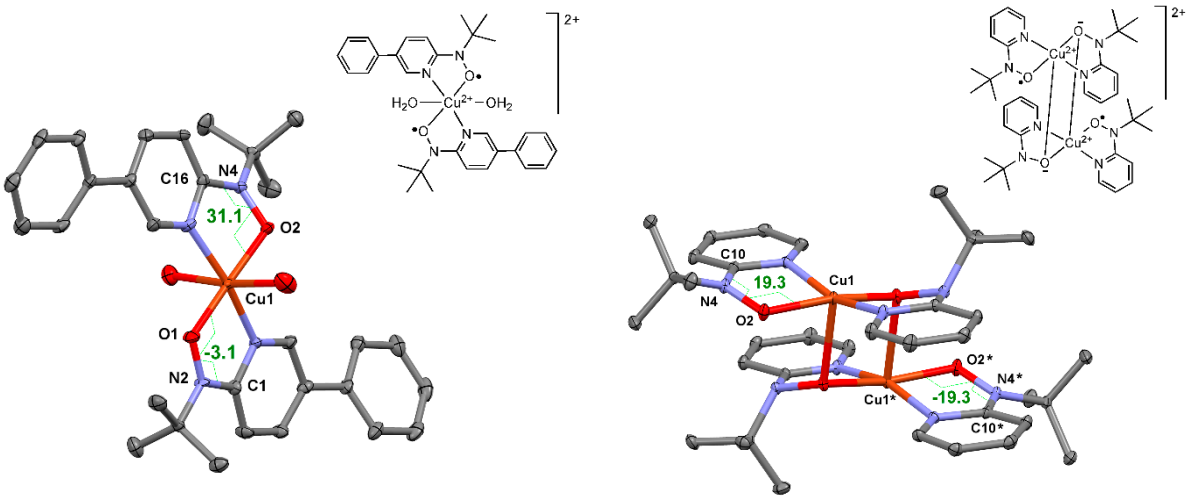

(**a**) (**b**)

Figure 10. X-ray crystal structures of the LS phase of (**a**) $[Cu(phpyNO)_2(H_2O)_2](BF_4)_2$ measured at 94 K and (**b**) $[\{Cu^{2+}(2pyNO\cdot)(\mu\text{-}2pyNO^-)\}_2](BF_4^-)_2$ at 50 K. Thermal ellipsoids are drawn at the 50% probability level. Counter anions and hydrogen atoms are omitted. Selected atomic numbering and torsion angles (φ (Ni–O–N–$C_{sp}{}^2$)) are indicated. Structural formulas are also shown. Adapted with permission from [111,112], published by the American Chemical Society, 2010.

Another example $[\{Cu^{2+}(2pyNO\cdot)(\mu\text{-}2pyNO^-)\}_2](BF_4^-)_2$ [112] (Figure 10b) behaved in a different manner. Despite a 4-centered dimerized structure, the magnetic behavior can be understood as a 2-centered monomer. A spin transition took place at 64 K. The spin structures of the low- and high-temperature phases are drawn as ↑-↑ and ↑-↓, respectively, for every spin pair. The space group remains *Pbca* across the transition, and the dimeric molecule keeps a centrosymmetry. In this case all the chelate ring deformations are synchronized, because S_{total} could be minimized to 0.

After combining the results on the nickel(II)– and copper(II)–nitroxide compounds, we obtain a clue to a driving force of this spin transition. The two Ni–O–N–$C_{sp}{}^2$ angular deformations in $[Ni(phpyNO)_2X_2]$ are synchronized, and both interactions alter from ferro- to antiferromagnetic on lowering temperature, because the spin multiplicity could reach

the minimum with $S_{total} = 0$. The present transition seems to be entropy-driven [71,113]; i.e., driven under the control of the change of spin entropy. The paramagnetic ligands play a crucial role in the motivation of the molecular deformation. It is a feasible experiment to mask the paramagnetic center by substituting a nitroxide group with a diamagnetic ketone group. In fact, Ovcharenko's group has clarified that the copper(II)-nitroxide complex showed the molecular spin transition while no structural rearrangement took place in the corresponding ketone analogue [114].

For detailed structural studies, a single-crystal-to-single-crystal-type transformation is welcomed [115], and such conditions are often realized in the present study. The entropy change due to the spin multiplicity change is generally small, and the spin entropy regulates the enthalpy term by Equation (11), leading to minimal atomic dislocation [116,117]. The plasticity of organic-based crystals is also important in accommodation of such structural modification.

In theory [35,118,119], the entropy difference of SCO can be calculated as a sum of contributions of electronic, vibrational, rotational, and translational terms (Equation (13)). In the solid state, two last terms are excluded. The electronic contribution comes from the degeneracy of each state as shown in Equation (14). When singlet and quintet states are involved, the electronic contribution is given as $R \ln 5 = 13.38$ J K^{-1} mol^{-1}.

$$\Delta S = \Delta S_{elec} + \Delta S_{vib} + \Delta S_{rot} + \Delta S_{trans} \quad (13)$$

$$\Delta S_{elec} = R \ln \frac{2S_{HS} + 1}{2S_{LS} + 1} \quad (14)$$

The experimental ΔS values are 26.3(1) and 24.0(7) J K^{-1} mol^{-1} for the Cl and Br compounds, respectively. These values are somewhat smaller than typical values for the iron(II) compounds similarly showing $S = 0 \rightleftarrows 2$ SCO [1,120]. The vibrational entropy contribution for the present compounds is almost negligible because the structural change is only the torsional deformation. This situation is completely different from that of the conventional one-centered SCO materials causing the drastic bond length change. Consequently, the small but substantial spin entropy change of the present compounds suffices the small enthalpy change of the structural transition.

The combined work from detailed magnetochemistry and structural chemistry afforded the evidence for the spin transition observed as an equilibrated solid-state reaction. Such reactions involve an intersystem-crossing nature and usually accompany the structural isomerization where the internal atomic geometries struggle to satisfy the spin state of each species.

2.5. Unfinished Spin-Transition Molecules

The stabilization of HS states raises $T_{1/2}$ while that of LS states lowers $T_{1/2}$ (Figure 1). The study on the chemical modification varying $T_{1/2}$ is important not only for exploring new materials but also for checking the validity of the molecular design and discussing the steric and electronic substituent effects which regulates the energy level of each state. The purpose of this section is to explain what happens in the pseudohalide case: X = NCS [121] and NCO [122]. The topic is focused on [Ni(phpyNO)$_2$(NCO)$_2$] (Figure 11).

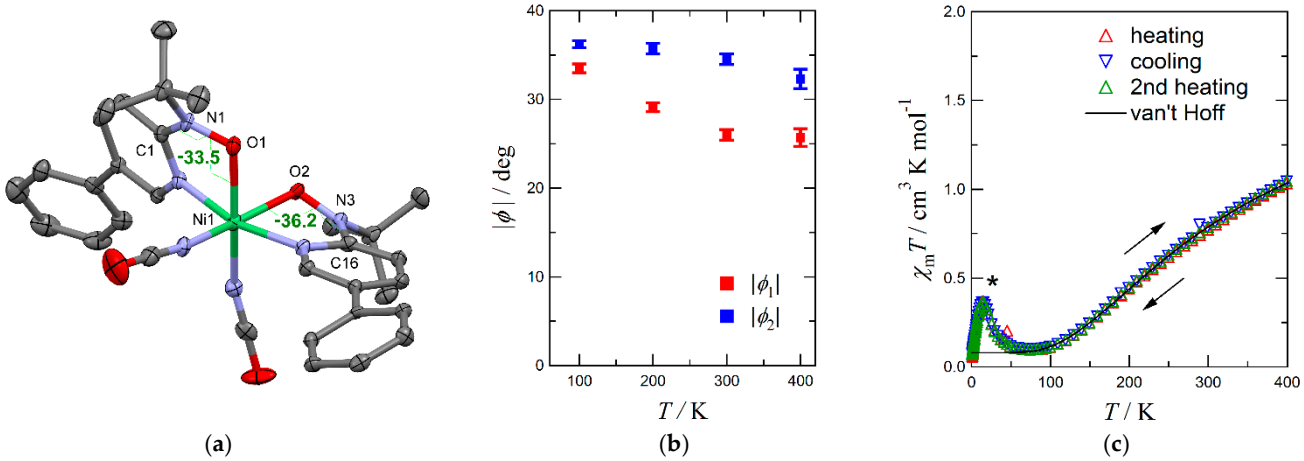

Figure 11. (**a**) X-ray crystal structure of [Ni(phpyNO)$_2$(NCO)$_2$] measured at 100 K. Hydrogen atoms are omitted. Thermal ellipsoids are drawn at the 50% probability level. Selected atomic numbering and torsion angles (φ (Ni–O–N–C$_{sp}{}^2$)) are indicated. (**b**) Temperature dependences of torsion angles ($|\varphi|$) and (**c**) χ_mT for [Ni(phpyNO)$_2$(NCO)$_2$]. An asterisk indicates impurity signal in (**c**). Adapted from [122], published by MDPI, 2020.

The torsion angles around Ni–O–N–C$_{sp}{}^2$ in [Ni(phpyNO)$_2$(NCO)$_2$] are 25.7(10) and 32.3(11)° at 400 K, indicating appreciable overlaps of the magnetic orbitals even at such a high temperature. On cooling, the torsion was enhanced as indicated with 33.5(5) and 36.2(4)° at 100 K (Figure 11a). However, the variation width is relatively narrow (Figure 11b), in comparison with those of the Cl and Br analogues (Section 2.4). All the observed torsion values 25.7(10)–36.2(4)° fell in the "antiferromagnetic region" in Figure 4.

The χ_mT value of [Ni(phpyNO)$_2$(NCO)$_2$] was practically null below ca. 100 K and gradually increased to 1.04 cm^3 K mol^{-1} on heating to 400 K (Figure 11c). A van't Hoff analysis was satisfactory like the X = Cl and Br derivatives, but $T_{1/2}$ was estimated as high as $\gg$ 400 K. The relatively large error of $T_{1/2}$ is unavoidable because it was derived only from the onset χ_mT data (the solid line in Figure 11c). Though $T_{1/2}$ seems to be somewhat overestimated, owing to a depopulation effect, [Ni(phpyNO)$_2$(NCO)$_2$] would undergo a possible spin transition at $T_{1/2} \gg 400$ K.

The parallel experiment and analysis on the NCS derivative, [Ni(phpyNO)$_2$(NCS)$_2$], indicated a spin transition with $T_{1/2}$ = 530(20) K [121]. The molecule crystallizes in an orthorhombic *Pbca* with Z = 8, but the space group was changed to a monoclinic $P2_1/n$ with Z = 8 in the low-temperature phase. The molecules are differentiated into two morphs on cooling. Such an order-disorder-type structural transition [123–125] as well as a molecular packing motif change [111,126] might certify the substantial spin transition.

It is convincing that the low-temperature phase is diamagnetic, but one may wonder if the high-temperature phase has the ground state of S_{total} = 2 or 1. The following notices strongly suggest that the ground state should be S_{total} = 2 in the high-temperature phase: (1) The driving force is needed for structural modification on both wings. (2) The estimated χ_mT value of the high-temperature phase was close to the S_{total} = 2 limit value.

To check the structure-dependence of the exchange coupling, the density functional theory (DFT) calculation was performed in Gaussian16 [127], using the determined atomic coordinates of [Ni(phpyNO)$_2$(NCO)$_2$]. The self-consistent field energies were calculated on the 100, 200, 300, and 400 K structures with the unrestricted B3LYP (Beck three-parameter hybrid functional combined with Lee–Yang–Parr correlation functional [128–130]) protocol and 6-311+G(2d,p) basis set. The B3LYP functional has been well-established for calculation of exchange couplings [131,132]. The broken symmetry method [133–135] was applied. According to this method, the ground state of the 100 K structure (Figure 11a) was singlet. The highest one was quintet with the singlet-quintet gap of −2196 K. Two triplet states, ↓-↑↑-↑ and ↑-↑↑-↓, intervene them. The ground state remained singlet at 400 K, but the gap was decreased. At the same time, the gap between the ground and first excited

triplet states also became as narrow as the thermal energy of the temperatures of magnetic measurements. All the calculation results are compatible with the experiments.

Full geometry optimization calculation provided a strong support for the exchange-coupling switch. The optimization on the diamagnetic LS and S_{total} = 2 HS states was conducted with the same protocol except for the 6-31+G(d) basis for organic elements. A model ligand methyl 2-pyridyl nitroxide (abbreviated as L′) was introduced to reduce calculation cost. As Figure 12a,b shows, the Ni–O–N–$C_{sp}{}^2$ torsion angles of diamagnetic [NiL′$_2$(NCO)$_2$] are 32.7°, and those of the S_{total} = 2 state are decreased to 11.9°. The calculation on the diamagnetic phase well reproduced the experimental values at 100 K, but the value of 11.9° was not found even at 400 K. This finding is acceptable by thinking that the 400 K form is transient toward the HS form.

Another calculation was performed on a model [NiL′$_2$Cl$_2$] for the spin-transition compound [Ni(phpyNO)$_2$Cl$_2$] [103] (Section 2.4). The geometries of the diamagnetic and S_{total} = 2 states were optimized on the same approximation and calculation level (Figure 12c,d, respectively). The former has φ = 35.4 and −27.2°, while the latter has φ = −9.3°. The calculation well reproduced the experimental LS geometries (38.9(2) and –29.2(2) at 85 K, Figure 9b) but still left a discrepancy from the experimental HS values (25.8(3) and 13.0(4) at 400 K, Figure 9b). The 400 K structure is a nearly but not ideal HS form.

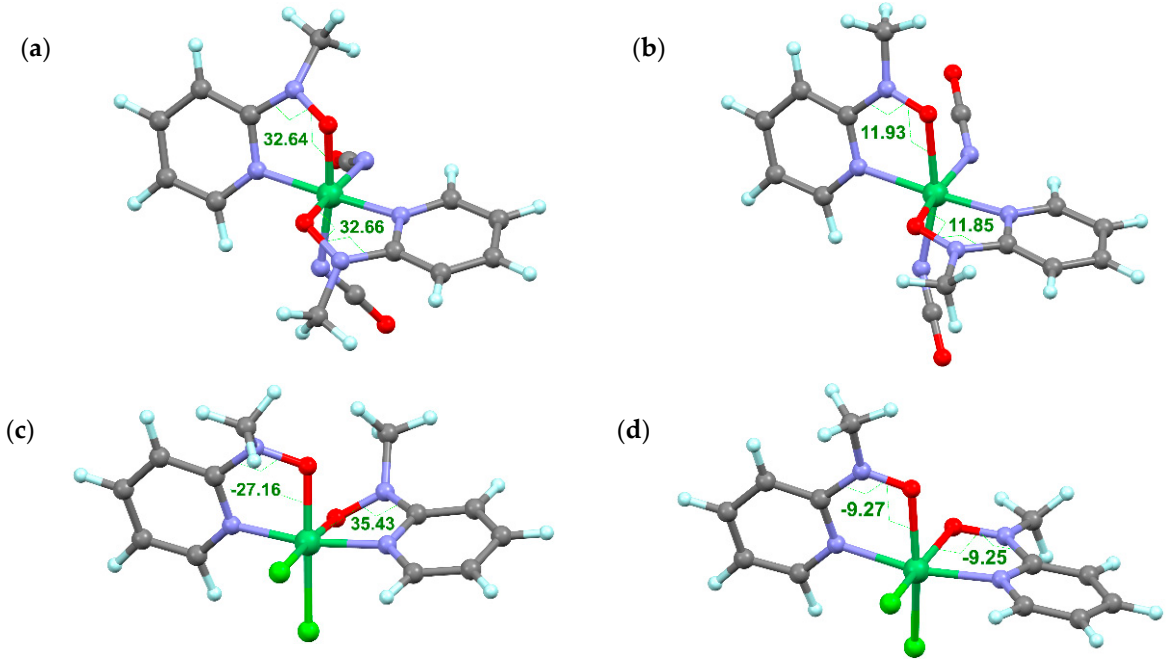

Figure 12. Optimized structures of 2p–3d–2p model compounds: [NiL′$_2$(NCO)$_2$] in the diamagnetic state (**a**) and the S_{total} = 2 state (**b**) and [NiL′$_2$Cl$_2$] in the diamagnetic state (**c**) and the S_{total} = 2 state (**d**), where L′ stands for methyl 2-pyridyl nitroxide. The Ni–O–N–$C_{sp}{}^2$ torsion angles are indicated. Color codes: Ni, green; C, black; H, turquoise; N, blue; O, red; Cl, light green. Adapted from [122], published by MDPI, 2020.

Figure 13a summarizes the DFT calculation results of the energy gaps on the X = NCO and NCS derivatives (this section) together with those of the X = Cl and Br analogues (Section 2.4). The singlet-quintet energy gaps were +102 and +141 K for the Cl and Br derivatives, respectively. In sharp contrast to the results on the NCO and NCS derivatives, the ground spin state of the Cl and Br ones was calculated as HS at 400 K.

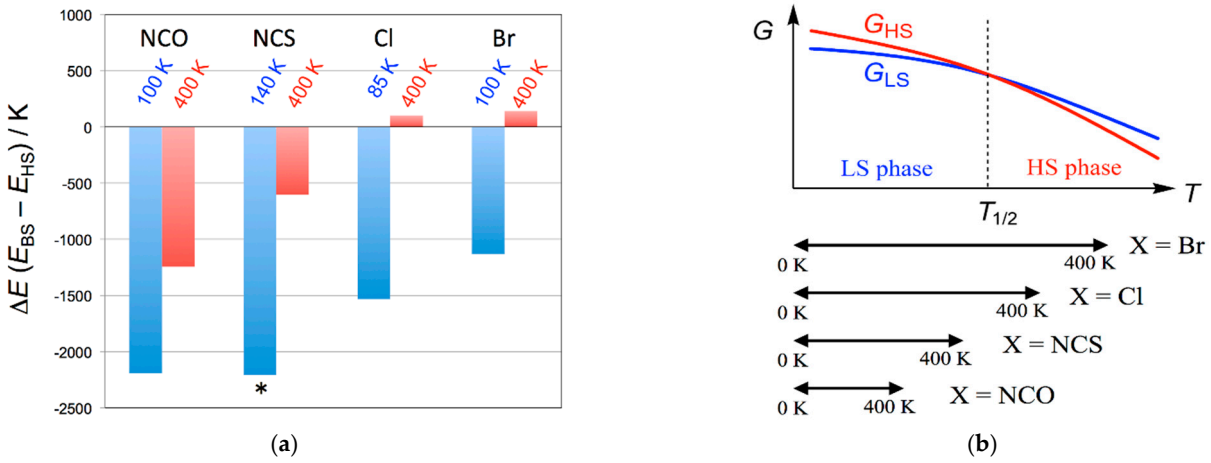

Figure 13. (**a**) Temperature dependence of the calculated energy gap between the broken-symmetry singlet state (BS) and quintet state (HS) on $[Ni(phpyNO)_2X_2]$ (X = NCO, NCS, Cl, Br). The temperatures where the structures were determined are noted. An asterisk indicates an averaged value of the independent molecules. (**b**) A schematic Gibbs energy diagram for $[Ni(phpyNO)_2X_2]$. The experimental windows are also shown in a lower panel. Adapted from [122], published by MDPI, 2020.

Overall, the four compounds are described in a common phase diagram (Figure 13b). The Cl and Br compounds undergo the energy level crossing, but the NCS and NCO compounds do not. The X = NCO and NCS derivatives are assumed to be a "pseudo spin-transition" material [52], or more correctly an "unfinished spin-transition" material, as a result of $T_{1/2}$ located beyond the upper limit of the experimental temperature (Figure 7). The spin transition is registered but unfinished to give a small HS fraction value. As for the Cl and Br compounds, $T_{1/2}$ is located inside the experimental temperature window, and "genuine spin-transition" compounds are materialized. In any case, when heated above $T_{1/2}$, the experimental susceptibility hardly reached the theoretical HS value but approached the paramagnetic one, due to the depopulation effect pronounced in high temperatures. We have to stress that a single-point X-ray crystallographic analysis could not reveal such a hidden structural transition.

In comparison among the four $[Ni(phpyNO)_2X_2]$ derivatives, the order is summarized as $T_{1/2}(Br) < T_{1/2}(Cl) < T_{1/2}(NCS) < T_{1/2}(NCO)$ (Figure 13b). The van der Waals radii of Br, Cl, and N have an inverse order [136], suggesting that the ligating atom mainly affects the steric congestion. Bulky coligands cannot accommodate out-of-plane displacement of the adjacent chelate ring atoms, so that bulkiness stabilizes the HS state and consequently reduces $T_{1/2}$.

2.6. Low-Spin Molecules

As noted in Section 2.2, nickel(II)-2pyNN complexes usually display a nonplanar 6-membered chelate ring and antiferromagnetic coupling. This hypothesis is tested with the following examples. The M/L = 1/1 compound $[Ni(2pyNN)(hfac)_2]$ showed antiferromagnetic coupling with $2J/k_B = -488$ K and $\varphi(Ni–O–N–C_{sp}{}^2) = 43.0°$ [83], where hfac stands for 1,1,1,5,5,5-hexafluoropentane- 2,4-dionate. This φ value belongs to the antiferromagnetic category according to the magneto-structural relationship (Figure 4). The 2-pyrazinyl-, 2-quinozalinyl-, 2-pyrimidinyl-, and 4-pyrimidinyl-substituted NN radicals are known, and to the best of our knowledge, their copper(II) and nickel(II) chelate complexes have been reported to exhibit all antiferromagnetic coupling [137–140], except for those involving the axial coordination to the copper(II) ion. The observation of ferromagnetic interaction in the radical copper wheels $[CuX_2(4PMNN)]_6$ (4PMNN = 4-pyrimidinyl NN; X = Cl, Br) [141,142] is rationalized because the chelate ring has the radical oxygen atom located at the axial site of the copper(II) coordination sphere.

The following will be of interest from the viewpoint of supramolecular chemistry. Another ground-low-spin example is relatively rare M/L = 3/6 compounds, $[Ni_3(pzNN)_6]$

and $[Ni_3(pzIN)_6]$ [143], where HpzNN and HpzIN are 3-pyrazolyl NN and 3-pyrazolyl IN, respectively (Figure 14a,b). A *meso*-helicate [144,145] (or mesocate [146]) structure is characterized. Namely, the opposite chirality around the inversion center at the central ion leads to a *meso*-helical symmetry as the whole molecule. For the pzNN compound, a half molecule is a crystallographically independent in a monoclinic $P2_1/n$ space group. The averaged φ(Ni–O–N–$C_{sp}{}^2$) was 35.0(7)°. For the pzIN compound, the IN oxygen atom is ligated to the nickel ion, giving a 6-membered chelate structure. There are two polymorphs. One morph has an intrinsic three-fold symmetry with respect to the molecular long axis in a cubic $Pa\bar{3}$ space group. A sixth molecule is crystallographically independent, and the unique φ was 38.0(5)°. The other morph is practically isomorphous to the pzNN derivative. The averaged φ was 43(5)°.

The magnetic susceptibility data (Figure 14c) were analyzed after inter-site interaction was approximately introduced as a mean-field approximation, giving the 3d–2p couplings, $2J/k_B = -80(2)$ and $-106(6)$ K, for the pzNN and pzIN compounds, respectively. The $\chi_m T$ vs. T profiles show a considerable convex, being consistent with the relatively small antiferromagnetic couplings. The stronger exchange interaction is observed in the latter than in the former, in good agreement with the larger φ of the latter. The finding is again reasonable, according to the magneto-structural relationship (Figure 4).

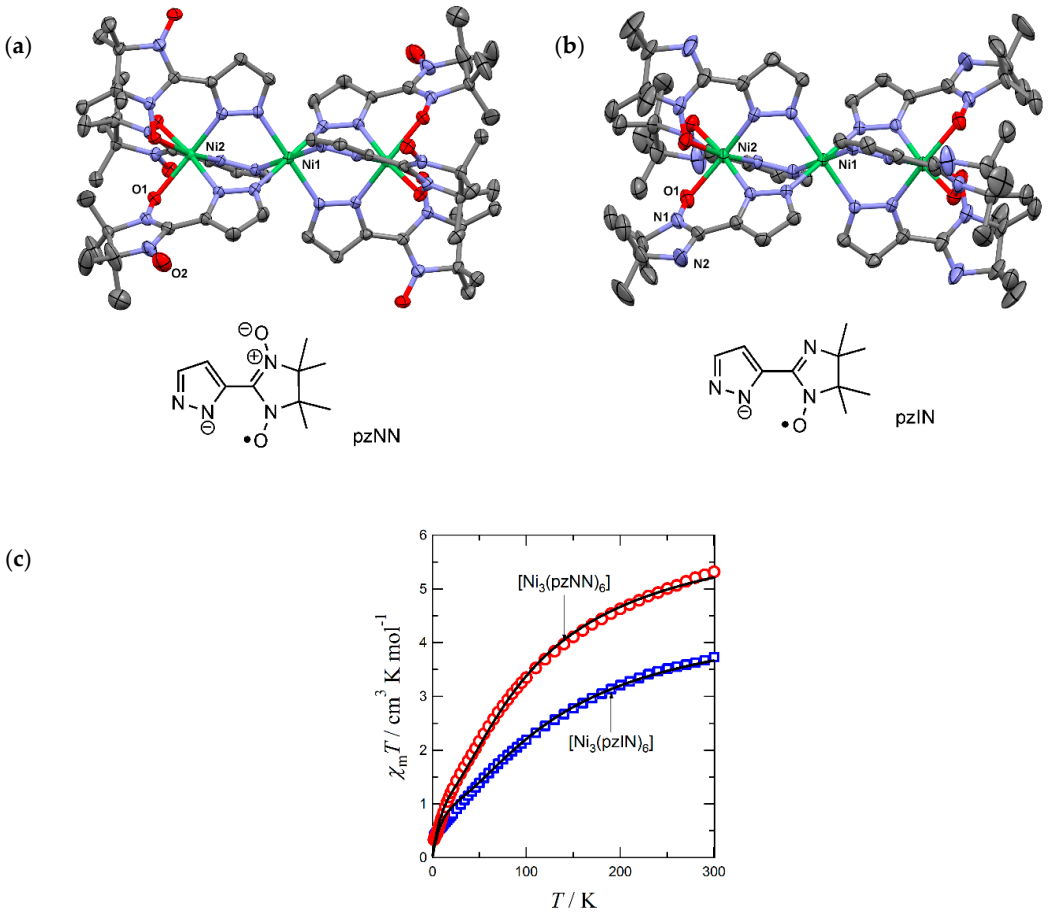

Figure 14. Molecular structures of (**a**) $[Ni_3(pzNN)_6]$ and (**b**) $[Ni_3(pzIN)_6]$ ($Pa\bar{3}$ phase) with thermal ellipsoids at the 50% probability level. Solvent molecules and hydrogen atoms are omitted. Selected atomic numberings are indicated. The structural formulas of paramagnetic ligands are also shown. (**c**) Temperature dependence of $\chi_m T$ for the two compounds. The solid lines represent calculated curves. Adapted with permission from [143], published by the Royal Society of Chemistry, 2006.

This supramolecular architecture was reproduced after replacing paramagnetic ligands with diamagnetic ones [114,147–149]. This method simplifies the magnetic analysis. Using a diamagnetic ligand HpzNTR (*N*-*tert*-butyl-α-3-pyrazolylnitrone), the trinuclear nickel(II,II,II) as well as iron(II,III,II) compounds were prepared, and their magnetic properties including triply pyrazolate-bridged superexchange interaction were investigated in detail [150].

2.7. Diamagnetic Molecules

Non-chelatable ligands are available, which would give rise to further twisted coordination structures. Taking a model complex of phNO (Figure 5) for example, a large angular torsion is expected from the steric repulsion between the nickel(II) ion and adjacent phenyl *ortho*–CH group (Figure 15a). A problem occurs in the stability of coordination compounds consisting of a monodentate ligand as well as the ligand itself. To solve these issues, we have employed a biradical ligand, tbpbNO (Figure 5), known as a ground triplet molecule [151]. The novelty of this work is that [{Ni(μ-tbpbNO)(hfac)$_2$}$_2$] showed a record strong exchange coupling [152], though the molecular skeleton is already known for the manganese(II) [153,154] and cobalt(II) complexes [155]. The hfac coligand was utilized because of a powerful accepting nature capable of coordinating the nitroxide oxygen atom.

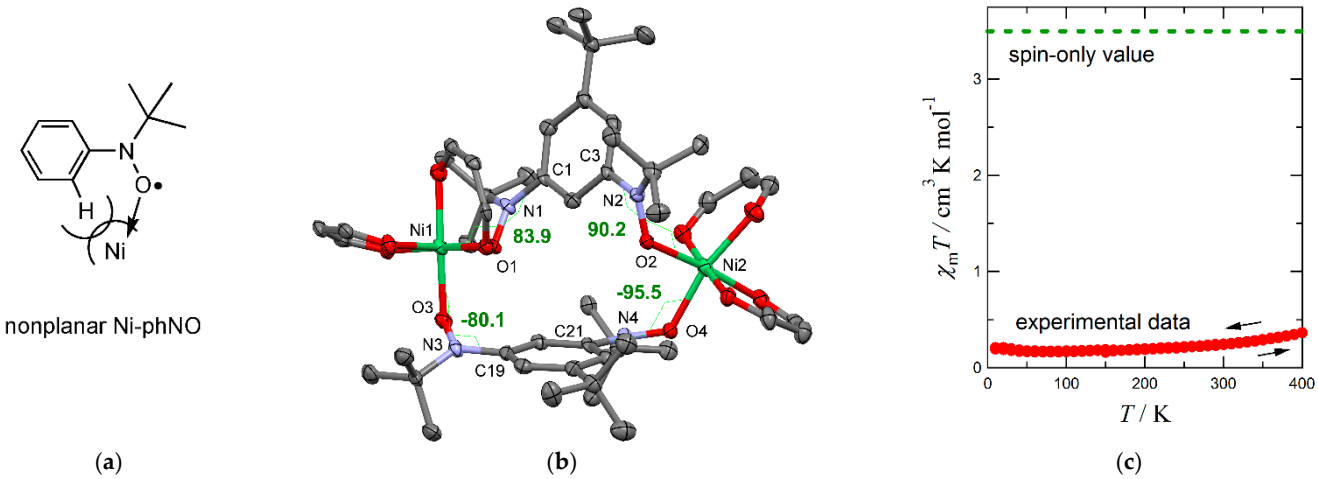

Figure 15. (**a**) Nonplanar Ni–O–N–$C_{sp}{}^2$ structure caused by a bulky phenyl group. (**b**) X-Ray crystal structure of [{Ni(μ-tbpbNO)(hfac)$_2$}$_2$] with thermal ellipsoids at the 50% probability level. Trifluloromethyl groups and hydrogen atoms are omitted. Selected atomic numbering and torsion angles (φ (Ni–O–N–$C_{sp}{}^2$)) are indicated. (**c**) Temperature dependence of $\chi_m T$ for [{Ni(μ-tbpbNO)(hfac)$_2$}$_2$]. Adapted with permission from [152], published by the Chemical Society of Japan, 2020.

Two biradical ligands doubly bridge two octahedral nickel ions, constructing a 16-membered macrocycle (Figure 15b). The radical oxygen atoms are located at a *cis* position of each nickel(II) ion. The φ(Ni–O–N–$C_{sp}{}^2$) angles are extremely large: 83.9(4), 90.2(3), −80.1(4), and −95.5(4)°. Note that the right angle is ideal for the overlapped arrangement of the metal dσ and radical π* magnetic orbitals. As Figure 15c displays, the magnetic study clarified the almost diamagnetic nature. The experimental $\chi_m T$ value was essentially null below 300 K and reached to a 5.6% level of the theoretical spin-only value (3.50 cm^3 K mol^{-1} from two $S_{Ni}{}^{2+}$ and four S_{rad} centers) at 400 K.

For estimation of *J*, a simple extrapolation in Figure 4 is risky because the slope is related with a bonding contribution due to the magnetic orbital overlap, partly regulated by a cos(2φ) law [91]. Instead, a simulation work was performed. Each magnetic exchange coupling constant was estimated by means of DFT calculation [127] on the UB3LYP/6-311+G(2d,p) level. A simulated $\chi_m T$ vs. T curve was drawn on the MAGPACK program [156], using the spin Hamiltonian defined as a 6-centered macrocyclic model

(Equation (15)). The simulation curve approximately reproduced the experimental data, indicating $2J_{\text{Ni-rad}}/k_B$ = ca. −1300 to −1400 K.

$$\begin{aligned}\hat{H} = &-2J_{\text{Ni1}-\text{O1}}\hat{S}_{\text{Ni1}}\bullet\hat{S}_{\text{O1}} - 2J_{\text{O1}-\text{O2}}\hat{S}_{\text{O1}}\bullet\hat{S}_{\text{O2}} - 2J_{\text{Ni2}-\text{O2}}\hat{S}_{\text{Ni2}}\bullet\hat{S}_{\text{O2}} \\ &-2J_{\text{Ni2}-\text{O4}}\hat{S}_{\text{Ni2}}\bullet\hat{S}_{\text{O4}} - 2J_{\text{O3}-\text{O4}}\hat{S}_{\text{O3}}\bullet\hat{S}_{\text{O4}} - 2J_{\text{Ni1}-\text{O3}}\hat{S}_{\text{Ni1}}\bullet\hat{S}_{\text{O3}}\end{aligned} \quad (15)$$

Thus, we have found the largest-class torsion angles and antiferromagnetic coupling parameters in [{Ni(μ-tbpbNO)(hfac)$_2$}$_2$]. As described in Section 2.2, antiferromagnetic contribution in Equation (1) is overwhelmingly large in general. From Figures 14 and 15, the nickel(II)–nitroxide compounds showing moderate to very strong antiferromagnetic coupling can be realized according to the common logic as depicted in Figures 3 and 4. The open ligation (non-chelate) compounds are good examples for testing an antiferromagnetic extreme case. When the coupling is antiferromagnetic, a ferrimagnetic approach would be promising by using large and small spins.

2.8. Miscellaneous

Nitroxide radicals are well-known to mediate redox reactions and in particular catalyze oxidation reactions in the presence of suitable oxidants [157–159]. Hydroxylamines possess an acidic proton [160], and the corresponding deprotonated forms, aminoxylates, can serve as a ligand; the bridging ligand in [{Cu^{2+}(2pyNO·)(μ-2pyNO^-)}$_2$](BF_4^-)$_2$ [112] (Figure 10b) is typical. However, a single-electron transfer to a nitroxide can afford an aminoxylate as well. Here the nickel(II) complexes having reduced anionic ligands will be described.

We attempted to prepare the iodide analogue [Ni(phpyNO)$_2$I$_2$], but the characterized products were only [Ni(phpyNO)$_2$] and [Ni(phpyNO)$_2$]I$_3$, as shown in Figure 16a,b and Supplementary Materials. The N–O bond length is a fingerprint of the oxidation states of the N–O group, namely, >N^+ = O, >N–O·, and >N–O^-. The N–O bond length in [Ni(phpyNO)$_2$] is 1.397(2) Å, and those in [Ni(phpyNO)$_2$]I$_3$ are 1.353(3) and 1.366(3) Å, being much longer than a typical N–O length of nitroxides (1.29 Å in a free ligand; 1.30 Å in coordination compounds [74]) but very close to that of aminoxylates (1.40–1.42 Å [161–165]). Consequently, the present compounds can be assigned to a reduced form (i.e., phpyNO^-).

The nickel(II) ion in [Ni(phpyNO)$_2$] is square planar. The valence of the nickel ion in [Ni(phpyNO)$_2$]I$_3$ is suggested to be +3.25 from the bond valence sum analysis [166], and accordingly, the charge balance is satisfied as [Ni^{3+}(phpyNO^-)$_2$]I_3^-. At this stage, it is concluded that the nitroxide ligands can be reduced with iodide according to Equation (16).

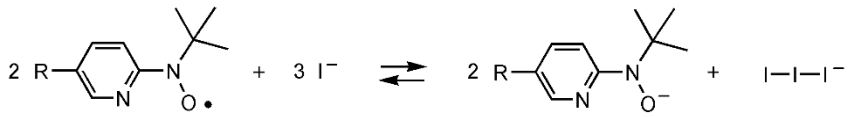

(16)

When tfpyNO [167] carrying a trifluoromethyl group (Figure 5) was applied, the reaction with nickel(II) chloride gave [Ni(tfpyNO)$_2$] (Figure 16c). The N–O bond length is 1.394(8) Å, which is close to that of [Ni(phpyNO)$_2$] and characterized to be anionic. Even after the purge of a reductant iodide, the electron-accepting trifluoromethyl group facilitates the reduction of the nitroxide group.

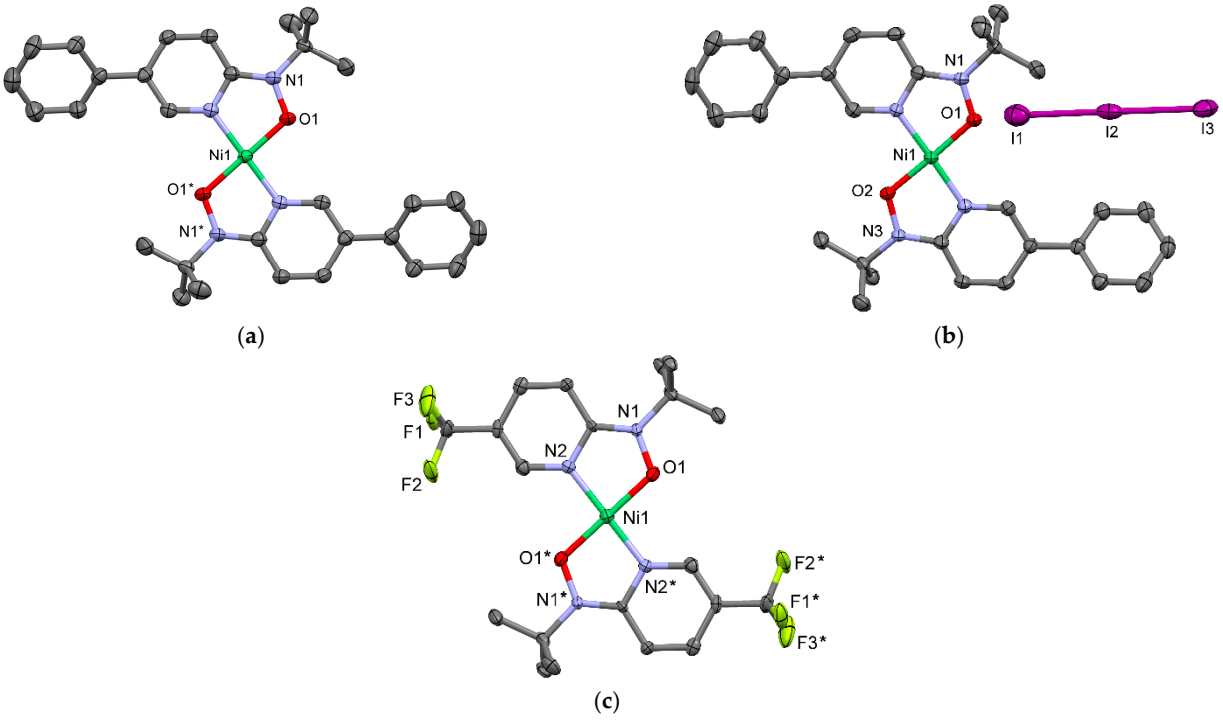

Figure 16. X-Ray crystal structures of (**a**) [Ni(phpyNO)$_2$], (**b**) [Ni(phpyNO)$_2$]I$_3$, (**c**) [Ni(tfpyNO$_2$)] with thermal ellipsoids at the 50% probability level. Hydrogen atoms are omitted. Selected atomic numbering is also shown. A half of molecule is crystallographically independent for (**a**) and (**c**).

The redox ability of the *tert*-butyl pyridyl nitroxides has been well investigated [161–165] and actually confirmed here. Charge-transfer-triggered switching materials, like valence–tautomeric cobalt(II)-SQ compounds [71–73] would be a next target of interest. It will be more promising to use manganese(II) instead of cobalt(II). Redox active Mn^{2+}–nitroxide complexes of this type have recently been described [168,169], but such properties have not yet been found for cobalt(II)-nitroxides, possibly because the value of the $Mn^{2+/3+}$ redox potential is more suitable for converting nitroxides into aminoxylates than that of $Co^{2+/3+}$.

Finally, a variety of the Ar–NO type ligands are briefly noted for possible applications in many directions. The 2py substituents can be replaced with diazaaromatic rings, and paramagnetic bridging ligands were designed and actually synthesized. Pyrimidine-4,6-bis(NO) (Figure 17) was proven to be a ground triplet molecule and applied to a linear trinuclear prototype for metal organic frameworks [170]. 4-X-Substituted pyridine-2,6-bis(NO) was a ground triplet molecule with $2J/k_B \gg +300$ K (X = mesityl [171], 9-anthryl, *tert*-butoxy [172]). A bulky stabilizing substituent X is required to be treated under ambient conditions. The pyridine bridge can be elongated with bi- and terpyridines, thus giving tetradentate bpy-bis(NO) [173,174] and pentadentate tpy-bis(NO) [175]. By using these paramagnetic ligands as a host, an exchange-coupling switch has been investigated with diamagnetic as well as paramagnetic guest ions. For pursuing ground triplet bridges, one of isomeric bpy-bis(NO) ligands, 3,4′-bipyridine-6,2′-diyl bis(*tert*-butyl nitroxide) (34bpy-bis(NO)), was synthesized [176]. The spin polarization mechanism [8,115,116,177–180] seems to hold for azaaromatic- and oligopyridine-bis(NO) systems.

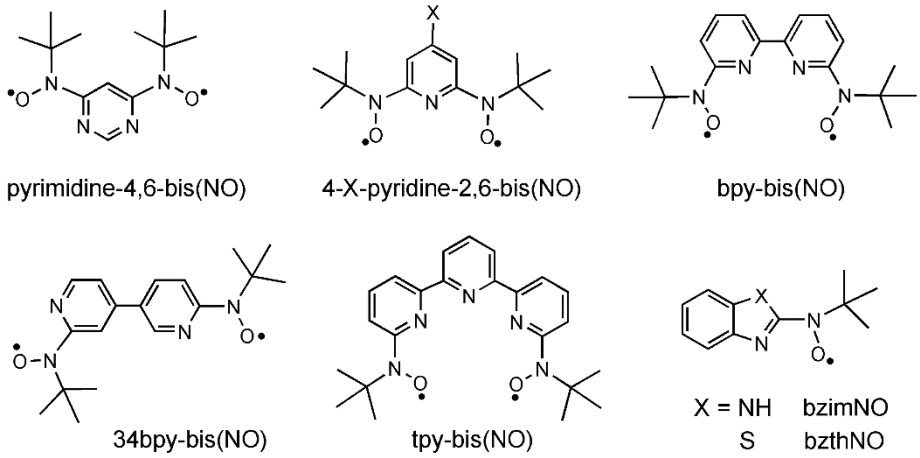

Figure 17. Structural formulas and abbreviations of 2-azaaryl *tert*-butyl nitroxides.

Lahti et al. have exploited benzimidazole- and benzothiazole-based isolable *tert*-butyl nitroxide compounds, bzimNO [181] and bzthNO [182], respectively, thanks to the stabilization from the electron delocalization. The imidazole and thiazole rings are smaller than the pyridine ring. This feature seems to be attracting, because, on chelate formation, the N and O bite angle of bzimNO and bzthNO might be open, being favorable for strong 3d–2p ferromagnetic coupling. Very recently, Luneau explained the spin-transition phenomenon of $[CuL_2(ClO_4)_2]$ (L = 2-imidazolyl-NN) [87] in terms of a magnetic coupling switch accompanied by the coordination structure modification [169]. This mechanism is quite similar to the present one and in particular to that of $[Cu(phpyNO)_2(H_2O)_2](BF_4)_2$ (Figure 10a) [111]. The small aromatic substituent seems to be beneficial for approaching the energy levels of the HS and LS states each other (see Section 2.2), even though it has a six-membered chelate ring.

3. Concluding Remarks

We have described a number of nickel(II)–nitroxide coordination complexes which show a broad spectrum from the ground HS molecules (Section 2.3) to the ground LS molecules (Sections 2.6 and 2.7) via the transient spin-transition molecules (Sections 2.4 and 2.5). Furthermore, the extensive researches on the ligand modification are concisely summarized (Section 2.8).

Molecular design must be provided on the basis of the reliable magneto-structural relationship, and the proposed relationship has been established by the cautious structural characterization and physical property analysis. The selection of a torsion angle φ (M–O–N–C_{sp^2}) is key to comprehend the geometry, propose a relationship, predict physical properties, and apply to molecular/crystal design and material production strategy. The torsion angle table is usually listed up in a crystallographic information file (.cif), and no recalculation is needed to assess φ. The φ parameter is handy, so that the plot of J vs. φ has also been applied to 4f–2p heterospin systems; for example, the Gd– [183–192], Tb– [193,194], and Dy–nitroxide compounds [195,196].

The ground HS (LS) molecules with a wide energy gap are characterized to be HS (LS) in the experimental temperature window. When the two energy levels are accidentally nearly degenerate, there is a chance of level crossing. The present structural transition or structural crossover originates in the equilibrated system regulated with the spin entropy. We almost always encountered the single-crystal-to-single-crystal structural transition/crossover in this project, thanks to the small atomic dislocation as well as the soft character of organic-based crystalline materials [197]. Though the structural change is small, the exchange coupling change is substantial because of the sensitive structure dependence. The single-point X-ray diffraction study cannot reveal a hidden transition. Combining work from magnetochemistry and structural chemistry as well as computational chemistry can tackle these problems.

The novelty of the present spin-transition mechanism lies in the ferro-/antiferromagnetic exchange-coupling switch, which is fully understood in terms of an equilibrated system (Figure 1). The spin state is determined by antiferro-/ferromagnetic contribution balance in multi-centered systems, in place of the aufbau/Hund balance in the conventional one-centered systems. In a molecular orbital picture, the aufbau principle works in gapped d-orbitals perturbed by a ligand field. Similarly, the aufbau principle also is operative in gapped bonding and antibonding orbitals caused by an orbital interaction. The HS electron configuration is favored under the control of Hund's rule in the one-centered SCO. This effect is also called intra-site ferromagnetic interaction or potential exchange [135,198,199]. The present spin-transition phenomena can be regarded as a multi-centered SCO.

As stated in the Introduction section, an advantage of our system is the use of strong ferromagnetic coupling, often stronger than the order of 300 K. It has been realized according to an appropriate molecular design based on the magneto-structural relationship. The large spin density at the ligating atom plays a crucial role to enhance the exchange coupling and sensitize the structural dependence of the exchange coupling, thus leading to the development of the multi-centered SCO materials. The structure-sensitive magnetic coupling is noticeable by referring a ferromagnetic limit ($2J/k_B$ = +409 K [74]) to an antiferromagnetic extreme ($2J/k_B \approx$ –1400 K [152]). For future work, this potential will be adopted to tuning of exchange coupling in 3d–2p heterospin materials by means of external stimulus.

Supplementary Materials: The following are available online at https://www.mdpi.com/2304-6740/9/2/10/s1. The CIF and the checkCIF output files are included in the Supplementary Materials. The experimental details and geometrical parameter tables can be obtained via http://www.ccdc.cam.ac.uk/conts/retrieving.html.

Author Contributions: Y.H. and Y.K. worked on the spin-transition materials using 2pyNO and related ligands. S.I. worked on the antiferromagnetic system using tbpbNO. T.I. supervised the project and wrote the manuscript. All authors have read and agreed to the published version of the manuscript.

Funding: This research was supported in part from JSPS KAKENHI (Scientific Research on Innovative Areas "Soft Crystals" JP17H06371 and Challenging Exploratory Research JP20K21170).

Acknowledgments: The authors are grateful to the colleagues whose names appeared as co-authors in the papers written in their laboratory, especially to Keita Osanai, Susumu Yamada, Chigusa Aoki, Kazuya Koide, Hinako Kawakami, Takuya Kanetomo (Tokyo University of Science, Japan), and Atsushi Okazawa (Nihon University, Japan).

Conflicts of Interest: The authors declare no competing financial interest.

References

1. Gütlich, P.; Goodwin, H.A. (Eds.) *Spin Crossover in Transition Metal Compounds I, II, and III*; Springer: Berlin, Germany, 2004.
2. Halcrow, M.A. (Ed.) *Spin-Crossover Materials: Properties and Applications*; John Wiley & Sons, Inc.: Oxford, UK, 2013.
3. Molnár, G.; Rat, S.; Salmon, L.; Nicolazzi, W.; Bousseksou, A. Spin Crossover Nanomaterials: From Fundamental Concepts to Devices. *Adv. Mater.* **2018**, *30*, 1703862. [CrossRef]
4. Coronado, E. Molecular magnetism: From chemical design to spin control in molecules, materials and devices. *Nat. Rev. Mater.* **2020**, *5*, 87–104. [CrossRef]
5. Kumar, K.S.; Ruben, M. Emerging trends in spin crossover (SCO) based functional materials and devices. *Coord. Chem. Rev.* **2017**, *346*, 176–205. [CrossRef]
6. Sato, O.; Tao, J.; Zhang, Y.Z. Control of magnetic properties through external stimuli. *Angew. Chem. Int. Ed.* **2007**, *46*, 2152–2187. [CrossRef] [PubMed]
7. Ratera, I.; Veciana, J. Playing with organic radicals as building blocks for functional molecular materials. *Chem. Soc. Rev.* **2012**, *41*, 303–349. [CrossRef] [PubMed]
8. Iwamura, H. What role has organic chemistry played in the development of molecule-based magnets? *Polyhedron* **2013**, *66*, 3–14. [CrossRef]
9. Caneschi, A.; Gatteschi, D.; Sessoli, R.; Rey, P. Toward molecular magnets: The metal–radical approach. *Acc. Chem. Res.* **1989**, *22*, 392–398. [CrossRef]
10. Meng, X.; Shi, W.; Cheng, P. Magnetism in one-dimensional metal–nitronyl nitroxide radical system. *Coord. Chem. Rev.* **2019**, *378*, 134–150. [CrossRef]

11. Faust, T.B.; D'Alessandro, D.M. Radicals in metal–organic frameworks. *RSC Adv.* **2014**, *4*, 17498–17512. [CrossRef]
12. Lü, B.; Chen, Y.; Li, P.; Wang, B.; Müllen, K.; Yin, M. Stable radical anions generated from a porous perylenediimide metal–organic framework for boosting near-infrared photothermal conversion. *Nat. commun.* **2019**, *10*, 1–8. [CrossRef]
13. Castellano, M.; Ruiz-García, R.; Cano, J.; Ferrando-Soria, J.; Pardo, E.; Fortea-Pérez, F.R.; Stiriba, S.-E.; Barros, W.P.; Stumpf, H.O.; Cañadillas-Delgado, L.; et al. Metallosupramolecular approach toward multifunctional magnetic devices for molecular spintronics. *Coord. Chem. Rev.* **2015**, *303*, 110–138. [CrossRef]
14. Kurmoo, M. Magnetic metal–organic frameworks. *Chem. Soc. Rev.* **2009**, *38*, 1353–1379. [CrossRef] [PubMed]
15. Thorarinsdottir, A.E.; Harris, T.D. Metal–Organic Framework Magnets. *Chem. Rev.* **2020**, *120*, 8716–8789. [CrossRef] [PubMed]
16. Kitazawa, T.; Gomi, Y.; Takahashi, M.; Takeda, M.; Enomoto, M.; Miyazaki, A.; Enoki, T. Spin-crossover behaviour of the coordination polymer $Fe^{II}(C_5H_5N)_2Ni^{II}(CN)_4$. *J. Mater. Chem.* **1996**, *6*, 119–121. [CrossRef]
17. Murphy, M.J.; Zenere, K.A.; Ragon, F.; Southon, P.D.; Kepert, C.J.; Neville, S.M. Guest programmable multistep spin crossover in a porous 2-D Hofmann-type material. *J. Am. Chem. Soc.* **2017**, *139*, 1330–1335. [CrossRef]
18. Takahashi, K.; Cui, H.B.; Okano, Y.; Kobayashi, H.; Mori, H.; Tajima, H.; Einaga, Y.; Sato, O. Evidence of the chemical uniaxial strain effect on electrical conductivity in the spin-crossover conducting molecular system: $[Fe^{III}(qnal)_2][Pd(dmit)_2]_5$·acetone. *J. Am. Chem. Soc.* **2008**, *130*, 6688–6689. [CrossRef]
19. Djukic, B.; Lemaire, M.T. Hybrid Spin-crossover conductor exhibiting unusual variable-temperature electrical conductivity. *Inorg. Chem.* **2009**, *48*, 10489–10491. [CrossRef]
20. Aromí, G.; Real, J.A. Special Issue "Spin Crossover (SCO) Research". *Magnetochemistry* **2016**, *2*, 28. [CrossRef]
21. Takahashi, K. Spin-Crossover Complexes. *Inorganics* **2018**, *6*, 32. [CrossRef]
22. Kitazawa, T. Synthesis and Applications of New Spin Crossover Compounds. *Crystals* **2019**, *9*, 382. [CrossRef]
23. Ovchinnikov, S.G. Spin Crossover (SCO) Research 2020. *Molecules* **2020**, *25*. Available online: https://www.mdpi.com/journal/molecules/special_issues/SCO_Research (accessed on 1 January 2021).
24. Hayami, S.; Holmes, S.M.; Halcrow, M.A. Spin-State Switches in Molecular Materials Chemistry. *J. Mater. Chem. C* **2015**, *3*, 7775–7778. [CrossRef]
25. Kimura, A.; Ishida, T. Spin-crossover temperature predictable from DFT calculation for iron(II) complexes with 4-substituted pybox and related heteroaromatic ligands. *ACS Omega* **2018**, *3*, 6737–6747. [CrossRef] [PubMed]
26. Kimura, A.; Ishida, T. Pybox-iron(II) spin-crossover complexes with substituent effects from the 4-position of the pyridine ring (Pybox= 2,6-Bis(oxazolin-2-yl)pyridine). *Inorganics* **2017**, *5*, 52. [CrossRef]
27. Yamasaki, M.; Ishida, T. Heating-rate dependence of spin-crossover hysteresis observed in an iron(II) complex having tris(2-pyridyl)methanol. *J. Mater. Chem. C* **2015**, *3*, 7784–7787. [CrossRef]
28. Hirosawa, N.; Oso, Y.; Ishida, T. Spin crossover and light-induced excited spin-state trapping observed for an iron(II) complex chelated with tripodal tetrakis(2-pyridyl)methane. *Chem. Lett.* **2012**, *41*, 716–718. [CrossRef]
29. Ishida, T.; Kanetomo, T.; Yamasaki, M. An iron(II) complex tripodally chelated with 1,1,1-tris(pyridin-2-yl)ethane showing room-temperature spin-crossover behaviour. *Acta Crystallogr. Sect. C Struct. Chem.* **2016**, *72*, 797–801. [CrossRef]
30. Ondo, A.; Ishida, T. Cobalt(II) terpyridin-4′-yl nitroxide complex as an exchange-coupled spin-crossover material. *Crystal* **2018**, *8*, 155. [CrossRef]
31. Mochida, N.; Kimura, A.; Ishida, T. Spin-Crossover Hysteresis of $[Fe^{II}(L_H{}^{iPr})_2(NCS)_2]$ ($L_H{}^{iPr}$ = *N*-2-Pyridylmethylene- 4-Isopropylaniline) Accompanied by Isopropyl Conformation Isomerism. *Magnetochemistry* **2015**, *1*, 17–27. [CrossRef]
32. Oso, Y.; Kanatsuki, D.; Saito, S.; Nogami, T.; Ishida, T. Spin-crossover Transition Coupled with Another Solid–Solid Phase Transition for Iron(II) Thiocyanate Complexes Chelated with Alkylated *N*-(Di-2-pyridylmethylene)anilines. *Chem. Lett.* **2008**, *37*, 760–761. [CrossRef]
33. Oso, Y.; Ishida, T. Spin-crossover transition in a mesophase iron(II) thiocyanate complex chelated with 4-hexadecyl-*N*-(2-pyridylmethylene)aniline. *Chem. Lett.* **2009**, *38*, 604–605. [CrossRef]
34. Boca, R. (Ed.) *Theoretical Foundations of Molecular Magnetism: Current Methods in Inorganic Chemistry*; Elsevier: Amsterdam, The Netherlands, 1999; Volume 1, pp. 541–563.
35. Cirera, J.; Via-Nadal, M.; Ruiz, E. Benchmarking density functional methods for calculation of state energies of first row spin-crossover molecules. *Inorg. Chem.* **2018**, *57*, 14097–14105. [CrossRef] [PubMed]
36. Olguín, J. Unusual metal centres/coordination spheres in spin crossover compounds. *Coord. Chem. Rev.* **2020**, *407*, 213148. [CrossRef]
37. Yamasaki, M.; Ishida, T. First Iron(II) spin-crossover complex with an N_5S coordination sphere. *Chem. Lett.* **2015**, *44*, 920–921. [CrossRef]
38. Likhtenshtein, G.I. (Ed.) *Nitroxides. Brief History, Fundamentals, and Recent Developments*; Springer: Cham, Switzerland, 2020.
39. Hicks, R.G. (Ed.) *Stable Radicals: Fundamentals and Applied Aspects of Odd- Electron Compounds*; Wiley: Chichester, UK, 2011.
40. Haugland, M.M.; Lovett, J.E.; Anderson, E.A. Advances in the synthesis of nitroxide radicals for use in biomolecule spin labelling. *Chem. Soc. Rev.* **2018**, *47*, 668–680. [CrossRef] [PubMed]
41. Klare, J.P.; Steinhoff, H.J. Spin labeling EPR. *Photosynth. Res.* **2009**, *102*, 377–390. [CrossRef] [PubMed]
42. Nishimaki, H.; Ishida, T. Organic two-step spin-transition-like behavior in a linear $S = 1$ array: 3′-methylbiphenyl-3,5-diyl bis(*tert*-butylnitroxide) and related compounds. *J. Am. Chem. Soc.* **2010**, *132*, 9598–9599. [CrossRef]

43. Kanetomo, T.; Ishida, T. Notably Strong Antiferromagnetic Interaction in a Methylene-bridged Bis(dihydrophenanthridin-*N*-oxyl). *Chem. Lett.* **2017**, *46*, 188–190. [CrossRef]
44. Kanetomo, T.; Ichihashi, K.; Enomoto, M.; Ishida, T. Ground Triplet Spirobiradical: 2,2′,7,7′-Tetra(*tert*-butyl)-9,9′(10*H*,10′*H*)-spirobiacridine-10,10′-dioxyl. *Org. Lett.* **2019**, *21*, 3909–3912. [CrossRef]
45. Koizumi, N.; Ishida, T. Forced proximity of nitroxide groups in pincer compounds with a xanthene spacer. *Tetrahedron Lett.* **2017**, *58*, 2804–2808. [CrossRef]
46. Ishida, T.; Shinozuka, K.; Kubota, M.; Ohashi, M.; Nogami, T. Fullerene spin label. Synthesis and characterization of the [60] fullerene-substituted TEMPO radical. *J. Chem. Soc. Chem. Commun.* **1995**, 1841–1842. [CrossRef]
47. Nogami, T.; Ishida, T.; Yasui, M.; Iwasaki, F.; Takeda, N.; Ishikawa, M.; Kawakami, T.; Yamaguchi, K. Proposed mechanism of ferromagnetic interaction of organic ferromagnets: 4-(arylmethyleneamino)-2,2,6,6-tetramethylpiperidin-1-oxyls and related compounds. *Bull. Chem. Soc. Jpn.* **1996**, *69*, 1841–1848. [CrossRef]
48. Ovcharenko, V.; Fokin, S.; Chubakova, E.; Romanenko, G.; Bogomyakov, A.; Dobrokhotova, Z.; Lukzen, N.; Morozov, V.; Petrova, M.; Petrova, M.; et al. A Copper−Nitroxide Adduct Exhibiting Separate Single Crystal-to-Single Crystal Polymerization−Depolymerization and Spin Crossover Transitions. *Inorg. Chem.* **2016**, *55*, 5853–5861. [CrossRef] [PubMed]
49. Fedin, M.V.; Verber, S.L.; Bagryanskaya, E.; Ovcharenko, V.I. Electron Paramagnetic Resonance of Switchable Copper-Nitroxide-Based Molecular Magnets: An Indispensable Tool for Intriguing Systems. *Coord. Chem. Rev.* **2015**, *289–290*, 341–356. [CrossRef]
50. Ovcharenko, V.I.; Maryunina, K.Y.; Fokin, S.V.; Tretyakov, E.V.; Romanenko, G.V.; Ikorskii, V.N. Spin transitions in non-classical systems. *Russ. Chem. Bull.* **2004**, *53*, 2406–2427. [CrossRef]
51. Lanfranc de Panthou, F.; Belorizky, E.; Calemczuk, R.; Luneau, D.; Marcenat, C.; Ressouche, E.; Turek, P.; Rey, P. A New Type of Thermally Induced Spin Transition Associated with an Equatorial ↔ Axial Conversion in a Copper(II)–Nitroxide Cluster. *J. Am. Chem. Soc.* **1995**, *117*, 11247–11253. [CrossRef]
52. Hirel, C.; Li, L.; Brough, P.; Vostrikova, K.; Pécaut, J.; Mehdaoui, B.; Bernard, M.; Turek, P.; Rey, P. New Spin-Transition-Like Copper(II)−Nitroxide Species. *Inorg. Chem.* **2007**, *46*, 7545–7552. [CrossRef]
53. Lanfranc de Panthou, F.; Luneau, D.; Musin, R.; Öhrström, L.; Grand, A.; Turek, P.; Rey, P. Spin-Transition and Ferromagnetic Interactions in Copper(II) Complexes of a 3-Pyridyl-Substituted Imino Nitroxide. Dependence of the Magnetic Properties upon Crystal Packing. *Inorg. Chem.* **1996**, *35*, 3484–3491. [CrossRef]
54. Kahn, O. *Molecular Magnetism*; VCH: New York, NY, USA, 1993.
55. Miller, J.S.; Gatteschi, D. Molecule-based magnets. *Chem. Soc. Rev.* **2011**, *40*, 3065–3066. [CrossRef]
56. Lemaire, M.T. Recent developments in the coordination chemistry of stable free radicals. *Pure Appl. Chem.* **2004**, *76*, 277–293. [CrossRef]
57. Ferrando-Soria, J.; Vallejo, J.; Castellano, M.; Martinez-Lillo, J.; Pardo, E.; Cano, J.; Castro, I.; Lloret, F.; Ruiz-Garcia, R.; Julve, M. Molecular magnetism, quo vadis? A historical perspective from a coordination chemist viewpoint. *Coord. Chem. Rev.* **2017**, *339*, 17–103. [CrossRef]
58. Rota, J.B.; Calzado, C.J.; Train, C.; Robert, V. Microscopic origins of the ferromagnetic exchange coupling in oxoverdazyl-based Cu(II) complex. *J. Chem. Phys.* **2010**, *132*, 154702. [CrossRef] [PubMed]
59. McConnell, H.M. Ferromagnetism in Solid Free Radicals. *J. Chem. Phys.* **1963**, *39*, 1910. [CrossRef]
60. Romero, F.M.; Ziessel, R.; Luneau, D. Structural control of ferromagnetic interactions in nickel(II) complexes based on a tetradentate biradical. *Chem. Commun.* **1998**, 551–552. [CrossRef]
61. Luneau, D.; Rey, P.; Laugier, J.; Fries, P.; Caneschi, A.; Gatteschi, D.; Sessoli, R. Nitrogen-bonded copper(II)–imino nitroxide complexes exhibiting large ferromagnetic interactions. *J. Am. Chem. Soc.* **1991**, *113*, 1245–1251. [CrossRef]
62. Luneau, D.; Rey, P.; Laugier, J.; Belorizky, E.; Cogne, A. Ferromagnetic behavior of nickel(II)–imino nitroxide derivatives. *Inorg. Chem.* **1992**, *31*, 3578–3584. [CrossRef]
63. Hicks, R.G.; Lemaire, M.T.; Thompson, L.K.; Barclay, T.M. Strong ferromagnetic and antiferromagnetic exchange coupling between transition metals and coordinated verdazyl radicals. *J. Am. Chem. Soc.* **2000**, *122*, 8077–8078. [CrossRef]
64. Hearns, N.G.; Preuss, K.E.; Richardson, J.F.; Bin-Salamon, S. Design and Synthesis of a 4-(2′-Pyridyl)-1,2,3,5-Dithiadiazolyl Cobalt Complex. *J. Am. Chem. Soc.* **2004**, *126*, 9942–9943. [CrossRef]
65. Rawson, J.M.; Alberola, A.; Whalley, A. Thiazyl radicals: Old materials for new molecular devices. *J. Mater. Chem.* **2006**, *16*, 2560–2575. [CrossRef]
66. Morgan, I.S.; Peuronen, A.; Hanninen, M.M.; Reed, R.W.; Clérac, R.; Tuononen, H.M. 1-Phenyl-3-(pyrid-2-yl)benzo[e][1,2,4]triazinyl: The first "Blatter Radical" for coordination chemistry. *Inorg. Chem.* **2014**, *53*, 33–35. [CrossRef]
67. Sidharth, T.N.S.; Nasani, R.; Gupta, A.; Sooraj, B.N.S.; Roy, S.; Mondal, A.; Konar, S. Reversal of magnetic exchange coupling between copper(II) and Blatter radical depending on the coordination environment. *Inorg. Chim. Acta* **2020**, *503*, 119395. [CrossRef]
68. Blatter, H.M.; Lukaszewski, H. A new stable free radical. *Tetrahedron Lett.* **1968**, *9*, 2701–2705. [CrossRef]
69. Kahn, O.; Prins, R.; Reedijk, J.; Thompson, J.S. Orbital symmetries and magnetic interaction between copper(II) ions and the *o*-semiquinone radical. Magnetic studies of (di-2-pyridylamine)(3,5-di-*tert*-butyl- *o*-semiquinonato)copper(II) perchlorate and bis(bis(3,5-di-*tert*-butyl-*o*-semiquinonato)copper(II)). *Inorg. Chem.* **1987**, *26*, 3557–3561. [CrossRef]
70. Benelli, C.; Dei, A.; Gatteschi, D.; Pardi, L. Synthesis, redox behavior, magnetic properties, and crystal structure of a nickel(II)-semiquinone adduct with an unusually strong ferromagnetic coupling. *Inorg. Chem.* **1988**, *27*, 2831–2836. [CrossRef]

71. Adams, D.M.; Dei, A.; Rheingold, A.L.; Hendrickson, D.N. Bistability in the [Co^{II}(semiquinonate)$_2$] to [Co^{III}(catecholate)(semiquinonate)] valence-tautomeric conversion. *J. Am. Chem. Soc.* **1993**, *115*, 8221–8229. [CrossRef]
72. Chaudhuri, P.; Verani, C.N.; Bill, E.; Bothe, E.; Weyhermüller, T.; Wieghardt, K. Electronic structure of bis(*o*-iminobenzosemiquino nato)metal complexes (Cu, Ni, Pd). The art of establishing physical oxidation states in transition-metal complexes containing radical ligands. *J. Am. Chem. Soc.* **2001**, *123*, 2213–2223. [CrossRef]
73. Pierpont, C.G. Studies on charge distribution and valence tautomerism in transition metal complexes of catecholate and semiquinonate ligands. *Coord. Chem. Rev.* **2001**, *216*, 99–125. [CrossRef]
74. Okazawa, A.; Nagaichi, Y.; Nogami, T.; Ishida, T. Magneto-structure relationship in copper(II) and nickel(II) complexes chelated with stable *tert*-butyl 5-phenyl-2-pyridyl nitroxide and related radicals. *Inorg. Chem.* **2008**, *47*, 8859–8868. [CrossRef]
75. Ali, A.; Dhar, D.; Barman, S.K.; Lloret, F.; Mukherjee, R. Nickel(II) complex of a hexadentate ligand with two *o*-iminosemiquinonato(1−) π-radical units and its monocation and dication. *Inorg. Chem.* **2016**, *55*, 5759–5771. [CrossRef]
76. Lemes, M.A.; Brunet, G.; Pialat, A.; Ungur, L.; Korobkov, I.; Murugesu, M. Strong ferromagnetic exchange coupling in a {Ni^{II}_4} cluster mediated through an air-stable tetrazine-based radical anion. *Chem. Commun.* **2017**, *53*, 8660–8663. [CrossRef]
77. Murugesu, M.; Mavragani, N.; Kitos, A.A.; Brusso, J.L. Enhancing magnetic communication between metal centres: The role of *s*-tetrazine based radicals as ligands. *Chem. Eur. J.* **2021**, in press. [CrossRef] [PubMed]
78. Woods, T.J.; Stout, H.D.; Dolinar, B.S.; Vignesh, K.R.; Ballesteros-Rivas, M.F.; Achim, C.; Dunbar, K.R. Strong ferromagnetic exchange coupling mediated by a bridging tetrazine radical in a dinuclear nickel complex. *Inorg. Chem.* **2017**, *56*, 12094–12097. [CrossRef] [PubMed]
79. Bonanno, N.M.; Lough, A.J.; Lemaire, M.T. Polynuclear Cu_4L_4 Copper(II) Aminyl Radical Coordination Complexes. *Inorg. Chem.* **2018**, *57*, 4837–4840. [CrossRef] [PubMed]
80. De Souza, M.S.; Briganti, M.; Reis, S.G.; Stinghen, D.; Bortolot, C.S.; Cassaro, R.A.A.; Guedes, G.P.; Da Silva, F.C.; Ferreira, V.F.; Novak, M.A.; et al. Magnetic Cationic Copper(II) Chains and a Mononuclear Cobalt(II) Complex Containing $[Ln(hfac)_4]^-$ Blocks as Counterions. *Inorg. Chem.* **2019**, *58*, 1976–1987. [CrossRef]
81. Bubnov, M.P.; Teplova, I.A.; Cherkasova, A.V.; Baranov, E.V.; Fukin, G.K.; Romanenko, G.V.; Bogomyakov, A.S.; Straikov, A.G.; Cherkasov, V.K. Metal-ligand ferromagnetic exchange interactions in heteroligand bis-*o*-semiquinonato nickel complexes with 2,2′-dipyridine and 1,10-phenanthroline. *Polyhedron* **2019**, *158*, 262–269. [CrossRef]
82. Richardson, P.F.; Kreilick, R.W. Copper Complexes with Free-Radical Ligands. *J. Am. Chem. Soc.* **1977**, *99*, 8183–8187. [CrossRef]
83. Luneau, D.; Risoan, G.; Rey, P.; Grand, A.; Caneschi, A.; Gatteschi, D.; Laugier, J. Transition metal derivatives of a chelating nitronyl nitroxide ligand. Nickel(II) and manganese(II) complexes. *Inorg. Chem.* **1993**, *32*, 5616–5622. [CrossRef]
84. Aoki, C.; Ishida, T.; Nogami, T. Metamagnetic behavior of $[Ni(4ImNNH)_2(NO_3)_2]$ having a ground high-spin state (4ImNNH = 4-imidazolyl nitronyl nitroxide). *Inorg. Chem. Commun.* **2003**, *6*, 1122–1125. [CrossRef]
85. Aoki, C.; Ishida, T.; Nogami, T. Molecular metamagnet $[Ni(4ImNNH)_2(NO_3)_2]$ (4ImNNH= 4-imidazolyl nitronyl nitroxide) and the related compounds showing supramolecular H-bonding interactions. *Inorg. Chem.* **2003**, *42*, 7616–7625. [CrossRef]
86. Luneau, D.; Rey, P. Magnetism of metal–nitroxide compounds involving bis-chelating imidazole and benzimidazole substituted nitronyl nitroxide free radicals. *Coord. Chem. Rev.* **2005**, *249*, 2591–2611. [CrossRef]
87. Yoshioka, N.; Irisawa, M.; Aizawa, N.; Aoki, T.; Inoue, H.; Ohba, S. Structure and magnetic property of 2-imidazolylnitronyl nitroxide and its metal complexes. *Mol. Cryst. Liq. Cryst. Sci. Technol. Sect. A* **1996**, *286*, 165–170. [CrossRef]
88. Okazawa, A.; Nogami, T.; Ishida, T. Strong intramolecular ferromagnetic couplings in nickel(II) and copper(II) complexes chelated with *tert*-butyl 5-methoxy-2-pyridyl nitroxide. *Polyhedron* **2009**, *28*, 1917–1921. [CrossRef]
89. Kyoden, Y.; Homma, Y.; Ishida, T. High-Spin and Incomplete Spin-Crossover Polymorphs in Doubly Chelated $[Ni(L)_2Br_2]$ (L = *tert*-Butyl 5-Phenyl-2-pyridyl Nitroxide). *Inorg. Chem.* **2019**, *58*, 10743–10755. [CrossRef]
90. Ondo, A.; Ishida, T. Structures and Magnetic Properties of Transition Metal Complexes Involving 2,2′-Bipyridin-6-yl Nitroxide. *AIP Conf. Proc.* **2017**, *1807*, 020023.
91. Okazawa, A. Magneto-Structural Relationship on Strong Exchange Interactions between Chelating Nitroxide Radical and Transition-Metal Spins. *IOP Conf. Ser. Mater. Sci. Eng.* **2017**, *202*, 012002. [CrossRef]
92. Venkataraman, L.; Klare, J.E.; Nuckolls, C.; Hyberstsen, M.S.; Steigerwald, M.L. Dependence of single-molecule junction conductance on molecular conformation. *Nature* **2006**, *442*, 904–907. [CrossRef]
93. Itoh, K.; Kinoshita, M. (Eds.) *Molecular Magnetism—New Magnetic Materials–Chapter 2*; Kodansha-Gordon and Breach: Tokyo, Japan, 2000.
94. Mallah, T.; Thiébaut, S.; Verdaguer, M.; Veillet, P. High-T_c molecular-based magnets: Ferrimagnetic mixed-valence chromium(III)-chromium(II) cyanides with T_c at 240 and 190 Kelvin. *Science* **1993**, *262*, 1554–1557. [CrossRef] [PubMed]
95. Kahn, O.; Charlot, M.F. Overlap density in binuclear complexes; a topological approach of the exchange interaction. In *Quantum Theory of Chemical Reactions*; Springer: Dordrecht, the Netherlands, 1980; pp. 215–240.
96. Osanai, K.; Okazawa, A.; Nogami, T.; Ishida, T. Strong Ferromagnetic Exchange Couplings in Copper(II) and Nickel(II) Complexes with a Paramagnetic Tridentate Chelate Ligand, 2,2′-Bipyridin-6-yl *tert*-Butyl Nitroxide. *J. Am. Chem. Soc.* **2006**, *128*, 14008–14009. [CrossRef]
97. Okazawa, A.; Nogami, T.; Ishida, T. *tert*-Butyl 2-Pyridyl Nitroxide Available as a Paramagnetic Chelate Ligand for Strongly Exchange-Coupled Metal−Radical Compounds. *Chem. Mater.* **2007**, *19*, 2733–2735. [CrossRef]
98. Keana, J.F. Newer aspects of the synthesis and chemistry of nitroxide spin labels. *Chem. Rev.* **1978**, *78*, 37–64. [CrossRef]

99. Miller, J.S.; Epstein, A.J.; Reiff, W.M. Ferromagnetic molecular charge-transfer complexes. *Chem. Rev.* **1988**, *88*, 201–220. [CrossRef]
100. Lahti, P.M. Structure–property relationships for metal-free organic magnetic materials. *Adv. Phys. Org. Chem.* **2011**, *45*, 93–169.
101. Landee, C.P.; Turnbull, M.M. A gentle introduction to magnetism: Units, fields, theory, and experiment. *J. Coord. Chem.* **2014**, *67*, 375–439. [CrossRef]
102. Gruber, S.J.; Harris, C.M.; Sinn, E. Metal Complexes as Ligands. VI. Antiferromagnetic Interactions in Trinuclear Complexes Containing Similar and Dissimilar Metals. *J. Chem. Phys.* **1968**, *9*, 2183–2191. [CrossRef]
103. Homma, Y.; Ishida, T. A new S = 0 ⇄ S = 2 "Spin-crossover" scenario found in a Nickel(II) Bis(nitroxide) system. *Chem. Mater.* **2018**, *30*, 1835–1838. [CrossRef]
104. Lluncll, M.; Casanova, D.; Circra, J.; Bofill, J.M.; Alcmany, P.; Alvarez, S.; Pinsky, M.; Avnir, D. *SHAPE, v2.1*; University of Barcelona: Barcelona, Spain, 2005.
105. Hogue, R.W.; Singh, S.; Brooker, S. Spin crossover in discrete polynuclear iron(II) complexes. *Chem. Soc. Rev.* **2018**, *47*, 7303–7338. [CrossRef]
106. Halcrow, M.A. Structure:function relationships in molecular spin-crossover complexes. *Chem. Soc. Rev.* **2011**, *40*, 4119–4142. [CrossRef]
107. Sheppard, C.L.; Tandon, S.S.; Thompson, L.K.; Bridson, J.N.; Miller, D.O.; Handa, M.; Lloret, F. Polynuclear copper(II) complexes with μ_2-1,1-azide bridges. Structural and magnetic properties. *Inorg. Chim. Acta* **1996**, *250*, 227–239. [CrossRef]
108. Sánchez-de-Armas, R.; Hernández, N.C.; Calzado, C.J. Copper–nitroxide based breathing crystals: A unified mechanism of gradual magnetostructural transition supported by quantum chemistry calculations. *Inorg. Chem. Front.* **2019**, *6*, 1228–1237. [CrossRef]
109. Kashiro, A.; Kohno, W.; Ishida, T. Odd–Even Effect on the Spin-Crossover Temperature in Iron(II) Complex Series Involving an Alkylated or Acyloxylated Tripodal Ligand. *Inorg. Chem.* **2020**, *59*, 10163–10171. [CrossRef]
110. Gütlich, P.; Gaspar, A.B.; Garcia, Y. Spin state switching in iron coordination compounds. *Beilstein J. Org. Chem.* **2013**, *9*, 342–391. [CrossRef] [PubMed]
111. Okazawa, A.; Ishida, T. Spin-Transition-Like Behavior on One Side in a Nitroxide–Copper(II)–Nitroxide Triad System. *Inorg. Chem.* **2010**, *49*, 10144–10147. [CrossRef] [PubMed]
112. Okazawa, A.; Hashizume, D.; Ishida, T. Ferro- and Antiferromagnetic Coupling Switch Accompanied by Twist Deformation around the Copper(II) and Nitroxide Coordination Bond. *J. Am. Chem. Soc.* **2010**, *132*, 11516–11524. [CrossRef] [PubMed]
113. Letard, J.-F.; Real, J.A.; Moliner, N.; Gaspar, A.B.; Capes, L.; Cador, O.; Kahn, O. Light Induced Excited Pair Spin State in an Iron(II) Binuclear Spin-Crossover Compound. *J. Am. Chem. Soc.* **1999**, *121*, 10630–10631. [CrossRef]
114. Tretyakov, E.V.; Tolstikov, S.E.; Suvorova, A.O.; Polushkin, A.V.; Romanenko, G.V.; Bogomyakov, A.S.; Veber, S.L.; Fedin, M.V.; Stass, D.V. Crucial role of paramagnetic ligands for magnetostructural anomalies in "breathing crystals". *Inorg. Chem.* **2012**, *51*, 9385–9394. [CrossRef]
115. Chaudhary, A.; Mohammad, A.; Mobin, S.M. Recent advances in single-crystal-to-single-crystal transformation at the discrete molecular level. *Cryst. Growth Des.* **2017**, *17*, 2893–2910. [CrossRef]
116. Ishida, T. Moving Molecules in Crystalline Solids: Gradual Structure Transition and Spin Transition/ Crossover. *IOP Conf. Ser.: Mater. Sci. Engineer.* **2019**, *515*, 012001. [CrossRef]
117. Kashiro, A.; Kyoden, Y.; Okazawa, A.; Ishida, T. Moving Organic Molecules in Crystalline Solids: Gradual Structural Transition and Spin Transition/Crossover. *J. Synth. Org. Chem. Jpn.* **2019**, *77*, 684–695. [CrossRef]
118. Molnaŕ, G.; Mikolasek, M.; Ridier, K.; Fahs, A.; Nicolazzi, W.; Bousseksou, A. Molecular Spin Crossover Materials: Review of the Lattice Dynamical Properties. *Ann. Phys. (Berlin Ger.)* **2019**, *531*, 1900076. [CrossRef]
119. Valtiner, M.; Paulsen, H.; Weinberger, P.; Linert, W. Theoretical investigations of a series of [hexakis(1-(tetrazol-1-yl)alkane-N^4)iron(II)] bis(tetrafluoroborate) spin crossover complexes: Methyl- to pentyl substituted species in the approximation of free cations. *MATCH Commun. Math. Comput. Chem.* **2007**, *57*, 749–761.
120. Kepp, K.P. Theoretical study of spin crossover in 30 iron complexes. *Inorg. Chem.* **2016**, *55*, 2717–2727. [CrossRef]
121. Kyoden, Y.; Ishida, T. An indication of spin-transition accompanied by an order-disorder structural transformation in [Ni(phpyNO)$_2$(NCS)$_2$] (phpyNO = *tert*-butyl 5-phenyl-2-pyridyl nitroxide). *RSC Adv.* **2020**, *10*, 16009–16015. [CrossRef]
122. Kyoden, Y.; Ishida, T. A Hidden Coordination-Bond Torsional Deformation as a Sign of Possible Spin Transition in Nickel(II)-Bis(nitroxide) Compounds. *Molecules* **2020**, *25*, 3790. [CrossRef] [PubMed]
123. Ortega-Villar, N.; Muñoz, M.C.; Real, J.A. Symmetry breaking in iron(II) spin-crossover molecular crystals. *Magnetochem.* **2016**, *2*, 16. [CrossRef]
124. Griffin, M.; Shakespeare, S.; Shepherd, H.J.; Harding, C.J.; Létard, J.F.; Desplanches, C.; Goeta, A.E.; Howard, J.A.K.; Powell, A.K.; Mereacre, V.; et al. A Symmetry-Breaking Spin-State Transition in Iron(III). *Angew. Chem. Int. Ed.* **2011**, *50*, 896–900. [CrossRef]
125. Sheu, C.F.; Pillet, S.; Lin, Y.C.; Chen, S.M.; Hsu, I.J.; Lecomte, C.; Wang, Y. Magnetostructural Relationship in the Spin-Crossover Complex *t*-{Fe(abpt)$_2$[N(CN)$_2$]$_2$}: Polymorphism and Disorder Phenomenon. *Inorg. Chem.* **2008**, *47*, 10866–10874. [CrossRef]
126. Kashiro, A.; Some, K.; Kobayashi, Y.; Ishida, T. Iron(II) and 1,1,1-Tris(2-pyridyl)nonadecane Complex Showing an Order–Disorder-Type Structural Transition and Spin-Crossover Synchronized over Both Conformers. *Inorg. Chem.* **2019**, *58*, 7672–7676. [CrossRef]
127. Frisch, M.J.; Trucks, G.W.; Schlegel, H.B.; Scuseria, G.E.; Robb, M.A.; Cheeseman, J.R.; Scalmani, G.; Barone, V.; Petersson, G.A.; Nakatsuji, H.; et al. *Gaussian 16, Revision C.01*; Gaussian Inc.: Wallingford, CT, USA, 2019.

128. Becke, A.D. Density- functional thermochemistry. III. The role of exact exchange. *J. Chem. Phys.* **1993**, *98*, 5648–5652. [CrossRef]
129. Becke, A.D. Density-functional thermochemistry. V. Systematic optimization of exchange-correlation functionals. *J. Chem. Phys.* **1997**, *107*, 8554–8560. [CrossRef]
130. Lee, C.; Yang, W.; Parr, R.G. Development of the Colle-Salvetti correlation-energy formula into a functional of the electron density. *Phys. Rev. B* **1988**, *37*, 785. [CrossRef]
131. Neese, F. Prediction of molecular properties and molecular spectroscopy with density functional theory: From fundamental theory to exchange-coupling. *Coord. Chem. Rev.* **2009**, *253*, 526–563. [CrossRef]
132. Ruiz, E.; Cano, J.; Alvarez, S.; Alemany, P. Broken symmetry approach to calculation of exchange coupling constants for homobinuclear and heterobinuclear transition metal complexes. *J. Comput. Chem.* **1999**, *20*, 1391–1400. [CrossRef]
133. Noodleman, L. Valence bond description of antiferromagnetic coupling in transition metal dimers. *J. Chem. Phys.* **1981**, *74*, 5737–5743. [CrossRef]
134. Yamaguchi, K.; Kawakami, T.; Takano, Y.; Kitagawa, Y.; Yamashita, Y.; Fujita, H. Analytical and ab initio studies of effective exchange interactions, polyradical character, unpaired electron density, and information entropy in radical clusters $(R)_N$: Allyl radical cluster ($N = 2-10$) and hydrogen radical cluster ($N = 50$). *Int. J. Quantum Chem.* **2002**, *90*, 370–385. [CrossRef]
135. Ciofini, I.; Daul, C.A. DFT calculations of molecular magnetic properties of coordination compounds. *Cood. Chem. Rev.* **2003**, *238*, 187–209. [CrossRef]
136. Bondi, A.V. van der Waals Volumes and Radii. *J. Phys. Chem.* **1964**, *68*, 441–451. [CrossRef]
137. Fegy, K.; Vostrikova, K.E.; Luneau, D.; Rey, P. New nitroxide based molecular magnetic materials. *Mol. Cryst. Liq. Cryst. Sci. Technol. Sect. A* **1997**, *305*, 69–80. [CrossRef]
138. Wang, C.; Ma, Y.; Wang, Y.; Wang, Q.; Li, L.; Cheng, P.; Liao, D. A New Quinoxalinyl-Substituted Nitronyl Nitroxide Radical and its Five-Spin Cu^{II} and Four-Spin Mn^{II} Complexes: Syntheses, Crystal Structures, and Magnetic Properties. *Aust. J. Chem.* **2012**, *65*, 672–679. [CrossRef]
139. Wang, J.; Li, J.N.; Zhang, S.L.; Zhao, X.H.; Shao, D.; Wang, X.Y. Syntheses and magnetic properties of a pyrimidyl-substituted nitronyl nitroxide radical and its cobalt(II) complexes. *Chem. Commun.* **2016**, *52*, 5033–5036. [CrossRef]
140. Omata, J.; Ishida, T.; Hashizume, D.; Iwasaki, F.; Nogami, T. Radical-copper macrocycles and related compounds. *Mol. Cryst. Liq. Cryst.* **2002**, *376*, 455–462. [CrossRef]
141. Omata, J.; Ishida, T.; Hashizume, D.; Iwasaki, F.; Nogami, T. Radical-copper wheels: Structure and magnetism of hexanuclear hybrid arrays. *Inorg. Chem.* **2001**, *40*, 3954–3958. [CrossRef] [PubMed]
142. Ishida, T.; Omata, J.; Nogami, T. Host–guest chemistry of radical-copper wheels. A supramolecular control of magnetic exchange coupling. *Polyhedron* **2003**, *22*, 2133–2138. [CrossRef]
143. Yamada, S.; Yasui, M.; Nogami, T.; Ishida, T. Self-assembled meso-helicates of linear trinuclear nickel(II)–radical complexes with triple pyrazolate bridges. *Dalton Trans.* **2006**, 1622–1626. [CrossRef]
144. Albrecht, M. Catecholate-Based Helicates. *Eur. J. Inorg. Chem.* **2020**, 2227–2237. [CrossRef]
145. Ousaka, N.; Shimizu, K.; Suzuki, Y.; Iwata, T.; Itakura, M.; Taura, D.; Iida, H.; Furusho, Y.; Mori, T.; Yashima, E. Spiroborate-based double-stranded helicates: Meso-to-*racemo* isomerization and ion-triggered springlike motion of the *racemo*-helicate. *J. Am. Chem. Soc.* **2018**, *140*, 17027–17039. [CrossRef]
146. Caulder, D.L.; Raymond, K.N. The rational design of high symmetry coordination clusters. *J. Chem. Soc. Dalton Trans.* **1999**, 1185–1200. [CrossRef]
147. Kahn, M.L.; Sutter, J.P.; Golhen, S.; Guionneau, P.; Ouahab, L.; Kahn, O.; Chasseau, D. Systematic investigation of the nature of the coupling between a Ln(III) ion (Ln = Ce(III) to Dy(III)) and its aminoxyl radical ligands. Structural and magnetic characteristics of a series of $\{Ln(organic\ radical)_2\}$ compounds and the related $\{Ln(Nitrone)_2\}$ derivatives. *J. Am. Chem. Soc.* **2000**, *122*, 3413–3421.
148. Kanetomo, T.; Yoshii, S.; Nojiri, H.; Ishida, T. Single-molecule magnet involving strong exchange coupling in terbium(III) complex with 2,2′-bipyridin-6-yl *tert*-butyl nitroxide. *Inorg. Chem. Front.* **2015**, *2*, 860–866. [CrossRef]
149. Kanetomo, T.; Ishida, T. Luminescent single-ion magnets from Lanthanoid(III) complexes with monodentate ketone ligands. *AIP Conf. Proc.* **2016**, *1709*, 020015.
150. Mochizuki, T.; Nogami, T.; Ishida, T. Ferromagnetic Superexchange Coupling through a Diamagnetic Iron(II) Ion in a Mixed-Valent Iron(III, II, III) *meso*-Helicate. *Inorg. Chem.* **2009**, *48*, 2254–2259. [CrossRef]
151. Chiarelli, R.; Gambarelli, S.; Rassat, A. Exchange interactions in nitroxide biradicals. *Mol. Cryst. Liq. Cryst. Sci. Technol. Sect. A.* **1997**, *305*, 455–478. [CrossRef]
152. Ito, S.; Ishida, T. Practically Diamagnetic Macrocycle Consisting of Nickel–Biradical Heterospins with the Largest Out-of-Plane Torsion at Coordination Bonds. *Chem. Lett.* **2020**, *49*, 1062–1065. [CrossRef]
153. Görlitz, G.; Hayamizu, T.; Itoh, T.; Matsuda, K.; Iwamura, H. Synthesis, Structure, and Magnetic Properties of a Cyclic Dimer of Bis(hexafluoroacetylacetonato){1,3-bis(*N*-*tert*-butyl-*N*-oxylamino)-5-*tert*-butylbenzene}manganese(II). *Inorg. Chem.* **1998**, *37*, 2083–2085. [CrossRef]
154. Rabu, P.; Drillon, M.; Iwamura, H.; Görlitz, G.; Itoh, T.; Matsuda, K.; Koga, N.; Inoue, K. Exchange Coupling Parameters and Energy Levels for Cyclic Metal–Radical Complexes of Bis(hexafluoroacetylacetonato)manganese(II) with 5-*tert*-Butyl-1,3-phenylenebis(*N*-*tert*-butylaminoxyl) and (4-*N*-*tert*-Butyl-*N*-oxyamino)pyridine. *Eur. J. Inorg. Chem.* **2000**, 211–216. [CrossRef]
155. Numata, Y.; Inoue, K. Synthesis, crystal structure and magnetic properties of a cyclic dimer of $[\{Co(hfac)_2\}\cdot BNO^{t\text{-}Bu}]_2$. *J. Mag. Mag. Mater.* **2007**, *310*, 1847–1848. [CrossRef]

156. Borrás-Almenar, J.J.; Clemente-Juan, J.M.; Coronado, E.; Tsukerblat, B.S. MAGPACK[1] A package to calculate the energy levels, bulk magnetic properties, and inelastic neutron scattering spectra of high nuclearity spin clusters. *J. Comput. Chem.* **2001**, *22*, 985–991. [CrossRef]
157. Nutting, J.E.; Rafiee, M.; Stahl, S.S. Tetramethylpiperidine *N*-oxyl (TEMPO), phthalimide *N*-oxyl (PINO), and related *N*-oxyl species: Electrochemical properties and their use in electrocatalytic reactions. *Chem. Rev.* **2018**, *118*, 4834–4885. [CrossRef] [PubMed]
158. Siu, J.C.; Sauer, G.S.; Saha, A.; Macey, R.L.; Fu, N.; Chauviré, T.; Lancaster, K.M.; Lin, S. Electrochemical azidooxygenation of alkenes mediated by a Tempo–N_3 charge-transfer complex. *J. Am. Chem. Soc.* **2018**, *140*, 12511–12520. [CrossRef] [PubMed]
159. Wang, F.; Rafiee, M.; Stahl, S.S. Electrochemical Functional-Group-Tolerant Shono-type Oxidation of Cyclic Carbamates Enabled by Aminoxyl Mediators. *Angew. Chem. Int. Ed.* **2018**, *57*, 6686–6690. [CrossRef] [PubMed]
160. Mollin, J.; Kasparek, F.; Lasovsky, J. On the basicity of hydroxylamine and its derivatives. *Chem. Zvesti* **1975**, *1*, 39–43.
161. Kirsh, J.M.; Woodside, A.J.; Manor, B.C.; Carroll, P.J.; Rablen, P.R.; Graves, C.R. Synthesis and Characterization of $(pyNO^{-})_2GaCl$: A Redox-Active Gallium Complex. *Inorganics* **2018**, *6*, 50. [CrossRef]
162. Poitras, A.M.; Bogart, J.A.; Cole, B.E.; Carroll, P.J.; Schelter, E.J.; Graves, C.R. Synthesis and characterization of aluminum complexes of redox-active pyridyl nitroxide ligands. *Inorg. Chem.* **2015**, *54*, 10901–10908. [CrossRef]
163. Bogart, J.A.; Lewis, A.J.; Boreen, M.A.; Lee, H.B.; Medling, S.A.; Carroll, P.J.; Booth, C.H.; Schelter, E.J. A ligand field series for the 4f-block from experimental and DFT computed Ce(IV/III) electrochemical potentials. *Inorg. Chem.* **2015**, *54*, 2830–2837. [CrossRef] [PubMed]
164. Bogart, J.A.; Lewis, A.J.; Medling, S.A.; Piro, N.A.; Carroll, P.J.; Booth, C.H.; Schelter, E.J. Homoleptic Cerium(III) and Cerium(IV) Nitroxide Complexes: Significant Stabilization of the 4+ Oxidation State. *Inorg. Chem.* **2013**, *52*, 11600–11607. [CrossRef] [PubMed]
165. McSkimming, A.; Su, J.; Cheisson, T.; Gau, M.R.; Carroll, P.J.; Batista, E.R.; Yang, P.; Schelter, E.J. Coordination Chemistry of a Strongly-Donating Hydroxylamine with Early Actinides: An Investigation of Redox Properties and Electronic Structure. *Inorg. Chem.* **2018**, *57*, 4387–4394. [CrossRef]
166. Brese, N.E.; O'keeffe, M. Bond-valence parameters for solids. *Acta Crystallogr. B Struct. Sci.* **1991**, *47*, 192–197. [CrossRef]
167. Bogart, J.A.; Lee, H.B.; Boreen, M.A.; Jun, M.; Schelter, E.J. Fine-tuning the oxidative ability of persistent radicals: Electrochemical and computational studies of substituted 2-pyridylhydroxylamines. *J. Org. Chem.* **2013**, *78*, 6344–6349. [CrossRef]
168. Lannes, A.; Suffren, Y.; Tommasino, J.B.; Chiriac, R.; Toche, F.; Khrouz, L.; Molton, F.; Duboc, C.; Kieffer, I.; Hazemann, J.L.; et al. Room Temperature Magnetic Switchability Assisted by Hysteretic Valence Tautomerism in a Layered Two-Dimensional Manganese Radical Coordination Framework. *J. Am. Chem. Soc.* **2016**, *138*, 16493–16501. [CrossRef]
169. Luneau, D. Coordination Chemistry of Nitronyl Nitroxide Radicals Has Memory. *Eur. J. Inorg. Chem.* **2020**, 597–604. [CrossRef]
170. Homma, Y.; Okazawa, A.; Ishida, T. Ground triplet pyrimidine-4,6-diyl bis(*tert*-butyl nitroxide) as a paramagnetic building block for metal–organic frameworks. *Tetrahedron Lett.* **2013**, *54*, 3120–3123. [CrossRef]
171. Kawakami, H.; Tonegawa, A.; Ishida, T. A designed room-temperature triplet ligand from pyridine-2,6-diyl bis(*tert*-butyl nitroxide). *Dalton Trans.* **2016**, *45*, 1306–1309. [CrossRef] [PubMed]
172. Kawakami, H.; Tonegawa, A.; Ishida, T. Pyridine-2,6-diyl dinitroxides as room-temperature triplet ligands. *AIP Conf. Proc.* **2016**, *1709*, 020017.
173. Koide, K.; Ishida, T. Biradical chelating host 2,2′-bipyridine-6,6′-diyl bis(*tert*-butyl nitroxide) showing tunable exchange magnetic coupling. *Inorg. Chem. Commun.* **2011**, *14*, 194–196. [CrossRef]
174. Koide, K.; Ishida, T. 2,2′-Bipyridine-6,6′-diyl bisnitroxide as a paramagnetic host: Encapsulation of a zinc(II) ion. *Polyhedron* **2011**, *30*, 3034–3037. [CrossRef]
175. Konno, T.; Koide, K.; Ishida, T. A supramolecular switch between ground high-and low-spin states using 2,2′:6′,2″-terpyridine-6,6″-diyl bis(*tert*-butyl nitroxide). *Chem. Commun.* **2013**, *49*, 5156–5158. [CrossRef] [PubMed]
176. Okazawa, A.; Terakado, Y.; Ishida, T.; Kojima, N. A triplet biradical with double bidentate sites based on *tert*-butyl pyridyl nitroxide as a candidate for strong ferromagnetic couplers. *New J. Chem.* **2018**, *42*, 17874–17878. [CrossRef]
177. Gallagher, N.M.; Olankitwanit, A.; Rajca, A. High-spin organic molecules. *J. Org. Chem.* **2015**, *80*, 1291–1298. [CrossRef]
178. Barone, V.; Cacelli, I.; Ferretti, A.; Monti, S.; Prampolini, G. An integrated protocol for the accurate calculation of magnetic interactions in organic magnets. *J. Chem. Theory Comput.* **2011**, *7*, 699–706. [CrossRef]
179. Yoshitake, T.; Kudo, H.; Ishida, T. Thermally Activated Paramagnets from Diamagnetic Polymers of Biphenyl-3,5-diyl Bis(*tert*-butyl Nitroxides) Carrying Methyl and Fluoro Groups at the 2′-and 5′-Positions. *Crystals* **2016**, *6*, 30. [CrossRef]
180. Ishida, T.; Iwamura, H. Bis[3-*tert*-butyl-5-(*N*-oxy-*tert*-butylamino)phenyl] nitroxide in a quartet ground state: A prototype for persistent high-spin poly[(oxyimino)-1,3-phenylenes]. *J. Am. Chem. Soc.* **1991**, *113*, 4238–4241. [CrossRef]
181. Ferrer, J.R.; Lahti, P.M.; George, C.; Antorrena, G.; Palacio, F. Synthesis, crystallography, and magnetic properties of 2-*tert*-butylaminoxylbenzimidazole. *Chem. Mater.* **1999**, *11*, 2205–2210. [CrossRef]
182. Taylor, P.; Ghalsasi, P.; Lahti, P.M. Modulating spin delocalization in conjugated nitroxides: 2-(*N*-aminoxyl-*N*-*tert*-butyl)-benzothiazole. *Tetrahedron Lett.* **2004**, *45*, 6295–6298. [CrossRef]
183. Ishida, T.; Murakami, R.; Kanetomo, T.; Nojiri, H. Magnetic study on radical-gadolinium(III) complexes. Relationship between the exchange coupling and coordination structure. *Polyhedron* **2013**, *66*, 183–187. [CrossRef]
184. Ikegaya, N.; Kanetomo, T.; Murakami, R.; Ishida, T. Triply Radical-coordinated Gadolinium(III) Complex as a High-spin $S = 5$ Assembly. *Chem. Lett.* **2012**, *41*, 82–83. [CrossRef]

185. Kanetomo, T.; Ishida, T. Strongest exchange coupling in gadolinium(III) and nitroxide coordination compounds. *Inorg. Chem.* **2014**, *53*, 10794–10796. [CrossRef] [PubMed]
186. Kanetomo, T.; Yoshitake, T.; Ishida, T. Strongest Ferromagnetic Coupling in Designed Gadolinium(III)–Nitroxide Coordination Compounds. *Inorg. Chem.* **2016**, *55*, 8140–8146. [CrossRef] [PubMed]
187. Kanetomo, T.; Kihara, T.; Miyake, A.; Matsuo, A.; Tokunaga, M.; Kindo, K.; Nojiri, H.; Ishida, T. Giant Exchange Coupling Evidenced with a Magnetization Jump at 52 T for a Gadolinium-Nitroxide Chelate. *Inorg. Chem.* **2017**, *56*, 3310–3314. [CrossRef]
188. Nakamura, T.; Kanetomo, T.; Ishida, T. Strong Antiferromagnetic Interaction in a Gadolinium(III) Complex with Methoxy-TEMPO Radical: A Relation between the Coupling and the Gd–O–N Angle. *Inorg. Chem.* **2021**, *60*. [CrossRef]
189. Gupta, T.; Rajeshkumar, T.; Rajaraman, G. Magnetic exchange in {Gd^{III}–radical} complexes: Method assessment, mechanism of coupling and magneto-structural correlations. *Phys. Chem. Chem. Phys.* **2014**, *16*, 14568–14577. [CrossRef]
190. Zhu, M.; Li, C.; Wang, X.; Li, L.; Sutter, J.P. Thermal Magnetic Hysteresis in a Copper–Gadolinium–Radical Chain Compound. *Inorg. Chem.* **2016**, *55*, 2676–2678. [CrossRef] [PubMed]
191. Xi, L.; Han, J.; Huang, X.; Li, L. Nitronyl Nitroxide Biradical-Based Binuclear Lanthanide Complexes: Structure and Magnetic Properties. *Magnetochem.* **2020**, *6*, 48. [CrossRef]
192. Kanetomo, T.; Naoi, Y.; Enomoto, M. Gadolinium-Triradical Complex with Ground $S = 10$ State: Synthesis, Structural Characterization and Magnetic Studies. *Eur. J. Inorg. Chem.* **2021**, in press. [CrossRef]
193. Baker, M.L.; Tanaka, T.; Murakami, R.; Ohira-Kawamura, S.; Nakajima, K.; Ishida, T.; Nojiri, H. Relationship between torsion and anisotropic exchange coupling in a Tb^{III}–radical-based single-molecule magnet. *Inorg. Chem.* **2015**, *54*, 5732–5738. [CrossRef] [PubMed]
194. Kanetomo, T.; Yasui, M.; Ishida, T. Exchange-coupled terbium–radical complex Tb-phNO showing slow reversal of magnetization. *Polyhedron* **2017**, *136*, 30–34. [CrossRef]
195. Patrascu, A.A.; Calancea, S.; Briganti, M.; Soriano, S.; Madalan, A.M.; Cassaro, R.A.A.; Caneschi, A.; Totti, F.; Vaz, M.G.F.; Andruh, M. A chimeric design of heterospin 2p–3d, 2p–4f, and 2p–3d–4f complexes using a novel family of paramagnetic dissymmetric compartmental ligands. *Chem. Commun.* **2017**, *53*, 6504–6507. [CrossRef]
196. Xi, L.; Sun, J.; Li, H.; Han, J.; Huang, X.; Li, L. Chain versus Discrete Assembly of Nitronyl Nitroxide Radical-Lanthanide Complexes: Regulating Magnetization Dynamics by Modifying Coordination Symmetry. *Cryst. Growth Des.* **2020**, *20*, 3785–3794. [CrossRef]
197. Kato, M.; Ito, H.; Hasegawa, M.; Ishii, K. Soft crystals: Flexible response systems with high structural order. *Chem. Eur. J.* **2019**, *25*, 5105–5112. [CrossRef]
198. Bencini, A.; Gatteschi, D. *EPR of Exchange Coupled Systems*; Dover Pub. Inc.: Nineola, NY, USA, 2012; Chapter 1.
199. Anderson, P.W. Theory of magnetic exchange interactions: Exchange in insulators and semiconductors. *Solid State Phys.* **1963**, *14*, 99–214.